

---

1 We thank both referees for their constructive comments to which we reply below followed by the  
2 track changes version of the manuscript.  
3

#### 4 **Response to Referee 1's Comments**

##### 5 **General comments**

6 This manuscript is very interesting and valuable in developing a global accurate ET dataset.  
7 Currently, there are many global or regional ET datasets, but their performances vary across  
8 different regions. This manuscript provides an insightful approach in processing these datasets  
9 ensemble. However, there are many procedures to be clarified to inform the readers.

10  
11 » **Answer:** Thank you very much for your positive comments and suggestions which for sure  
12 significantly improved the manuscript.  
13

##### 14 **Major comments**

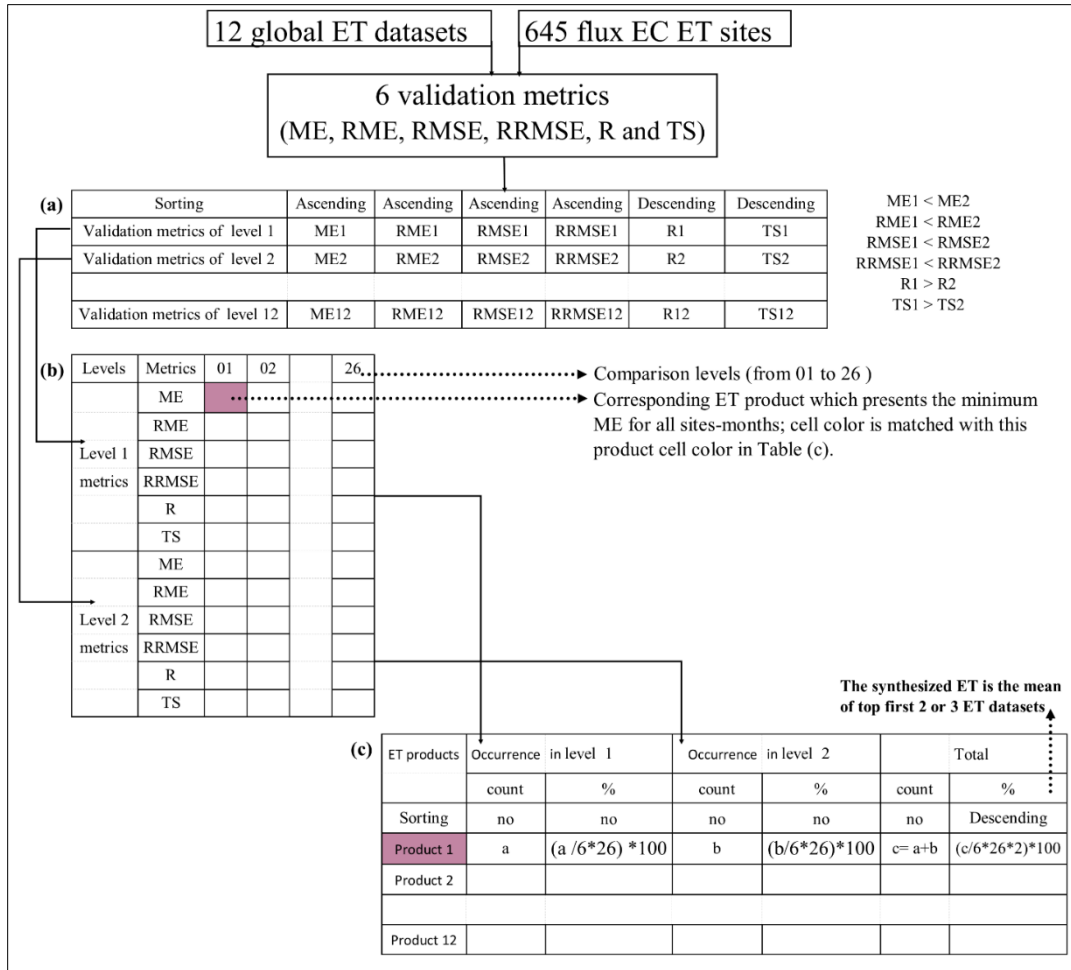
15  
16 I don't understand the meanings of "best first and second levels" and "levels one and two validation  
17 metrics". These two phrases have appeared many times and are vitally important to understand the  
18 synthesis procedure. If I understand this correctly, the performance metrics in Tables 5-8 were  
19 used to select two or three best ET datasets and the new dataset is produced by averaging these  
20 two or three datasets. A figure of processing procedure may be helping.  
21

22 » **Answer:** Thank you for pointing this out. The level one of validation metrics has the highest R  
23 and TS values and the lowest ME, RME, RMSE, and RRMSE while the level two of validation  
24 metrics has the highest R and TS values and the lowest ME, RME, RMSE, and RRMSE after level  
25 one. You are right, the performance metrics in **Tables 5-8** were used to select two or three best ET  
26 datasets and the new dataset is produced by averaging these two or three datasets. For that, **Fig. 1,**  
27 **that shown below,** was created to preview the synthesization method and is included in the revised  
28 manuscript under **Section 3.2.** Hence, we rewrote **Section 3.2** as follows:

29 "There are 6 validation metrics including R, TS, ME, RME, RMSE, and RRMSE. The  
30 validation values of 6 metrics are categorized into levels. The level one of validation metrics has  
31 the highest R and TS values and the lowest ME, RME, RMSE, and RRMSE while the level two  
32 of validation metrics has the highest R and TS values and the lowest ME, RME, RMSE, and  
33 RRMSE after level one. For that, R and TS sorted descending while ME, RME, RMSE, and  
34 RRMSE sorted ascending (**Fig.1a**) then the corresponding ET product of each validation metric  
35 saved in a new table to be used to fill in **Fig.1b.**

36 The current study proposes three steps to develop a synthesized global ET dataset. First,  
37 the ET datasets are compared based on 6 validated metrics to generate a matrix to indicate level  
38 one and two of the validation metrics of all ET products over all comparison levels (**Fig.1b**). For  
39 each level, there are 6 validation metrics in rows and 26 ET values of different time periods and  
40 underlying conditions in columns (comparison levels), including monthly average (01), annual  
41 average (02), monthly (January-December: 03-14), land cover types (15-19), climate classes (20-  
42 23), and elevation levels (24-26). Thus, the total number of cells is 156 for each level. Each cell in  
43 the matrix represents one of twelve ET products that belong to this level. Then, to select ET data  
44 for further synthesis, the number and percentage of ET product occurrence at matrix (**Fig.2b**) of  
45 level one and two were calculated (**Fig.1c**). ET products were ranked in descending order based

46 on the occurrence percentage of levels one and two (the last column in **Fig.1c**). Finally, the first  
 47 two or three highly ranked ET products were selected to incorporate into the ensemble ET. For  
 48 that, the selected ET products were resampled to a comparable spatial resolution if needed, and the  
 49 average was used as the synthesized ET value.”  
 50



51  
 52 **Fig.1.** Flowchart of the synthesis method.

53  
 54  
 55  
 56  
 57  
 58  
 59  
 60  
 61

---

62 The second major problem is the validation data. By reading this manuscript, it could be confirmed  
63 that the observed EC ET data serve as validation data in evaluating and ranking the 12 ET datasets  
64 and also the validation data in evaluating the proposed Global Actual Evapotranspiration dataset.  
65 There could be an overfitting effect. It is like we use the same dataset as calibration data and  
66 validation data at the same time. Therefore, a cross-checking method should be applied. For  
67 example, 2/3 of the EC sites be used to evaluate the ET datasets and 1/3 of EC sites to validate.  
68

69 » **Answer:** Thank you very much for your comment. You are right, it needs to split the in-situ data  
70 into 2 groups for calibration and validation. However, we do not calibrate ET products. We use in-  
71 situ data to see which one is performing better than others. Once ET products are selected, then  
72 we synthesize them into one and use in-situ data to validate to see if the synthesized data is better.  
73 Furthermore, From **Tables 1 and 3**, the flux EC ET sites, as well as the 12 ET products, are  
74 available in different periods. For evaluating each ET product the matched periods between EC  
75 sites and ET datasets were used (Xu et al. 2019; Li et al. 2018), that is why RME and RRMSE are  
76 included in the validation metrics. Further, the synthesized ET represented by the mean of PML  
77 and SSEBop about 60% (2003 to 2017) and the mean of NTSG and MOD16A2105 about 8%  
78 (2002-2002) indicating 68% of the synthesized ET are new data. For that, we used the matched  
79 period's method aiming to validate the new product under the same conditions of the experiment.  
80 We agreed with this method because we did not incorporate the flux EC ET data into the  
81 synthesized ET, it just serves as a ruler to prove to what extend each ET product works well in all  
82 comparison levels. Moreover, we used three regional ET datasets for comparison of consistent  
83 agreement over China, the United States, and the African continent to ensure the proposed product  
84 works well.  
85

86 Another question that should be discussed is the scale problem. The EC sites normally work in a  
87 very limited area and can only present the ET condition of a small region. The related uncertainty  
88 should be discussed in the manuscript.  
89

90 » **Answer:** Thank you for your very thoughtful comment. This is a common issue. The best way  
91 to validate the ET datasets is to use closure watershed water balances, however, these data set are  
92 quite a few. Flux EC ET data has its footprint, covering a larger area, but hard to match with a  
93 pixel. This issue still needs fundamental study. For that, we added **Lines 61-64**, as follows:

94 “Although flux EC ET is commonly flawed, particularly concerning energy balance  
95 closure at some sites (Foken, 2008; Helgason and Pomeroy, 2012), relatively short periods, and  
96 sparse spatial coverage, it is the most direct method for measuring the exchange between the  
97 surface and the atmosphere in different ecosystems (Foken et al., 2012; Baldocchi, 2014). Thus,  
98 site-pixel-level validation of certain ET products against flux EC ET as typically observed data  
99 has been performed by several studies in specific regions”

100  
101  
102  
103  
104  
105  
106  
107

---

108 **Minor comments**

109

110 Line 11: What do you mean by “they produce different levels of uncertainties?”

111 » **Answer:** Thank you for that comment. We rewrote the sentence (**Lines 9-11**) to be clearer, as  
112 follows:

113 “Although it is difficult to estimate ET over a large scale and for a long time, there are  
114 several global ET datasets available with uncertainty associated with various assumptions  
115 regarding their algorithms, parameters, and inputs”.

116

117 In the abstract, the synthesization method should be indicated clearly.

118 » **Answer:** Thank you for your cogent advice. We agree and have indeed done that (**Lines 12-15**),  
119 as follows:

120 “Through a site-pixel evaluation of 12 global ET products over different time periods, land  
121 surface types, and conditions, the high performing products were selected for synthesis of the new  
122 dataset using a high-quality flux eddy covariance covering the entire globe.”

123

124 Line 74: check the time period.

125 » **Answer:** Thank you for pointing this out. We changed “**1998-1995**” to “**1989-1995**”.

126

127 Line 258: the title of subplot c.

128 » **Answer:** Thank you for pointing this out. We changed RMSE (mm): (**d**) to RMSE (mm): (**c**).

129

130 Line 371-392: Different datasets were selected due to data availability. That means for each period,  
131 for example before 2003 and 2003-2017, different datasets were used. My concern is that the  
132 ensemble means/variations may differ greatly. An adjustment in the period mean/variation should  
133 be considered.

134

135 » **Answer:** Thank you for your very thoughtful comment. Although we agree with you, this time  
136 series adjustment is very important and should be done in the future. Therefore, we have added  
137 Lines **549-551**, as follows:

138 “since different datasets were selected due to data availability, also future improvements  
139 may be focused on the adjustment of the ensemble means particularly for longterm pixel-based  
140 studies.”

141

142 Some tables and figure captions are similar. For example, Table 5 and Table 12. The major  
143 differences between them are the time period, which should be clearly indicated.

144

145 » **Answer:** We appreciate your advice. Tables and figures caption has been revised (**Figures 6**  
146 **and 13; Tables 6-9, 12, 13**).

147

148

149

---

150 **Response to Referee 2's Comments**

151 The present article proposes a long-term synthesized ET product at a kilometer spatial resolution  
152 and monthly temporal resolution from 1982 to 2019. The authors made a trial application of GIS  
153 and remotely sensed data to reach the proposed aim of their study.

154  
155 » Answer: Thank you very much for your positive comments and suggestions which for sure  
156 significantly improved the manuscript.

157  
158 The presented article would be a good piece of work by supporting the conclusion with the  
159 obtained findings.

160  
161 » **Answer:** Thank you for your very thoughtful comment. We have added the obtained findings to  
162 the Conclusions section as follows:

163 ” The average annual ET from 1982–2019 is 567 mm year<sup>-1</sup>. Although no product  
164 performed better in terms of all selected validation criteria in all classification levels, PML,  
165 GLDAS20, SSEBop, MOD16A2105, GLDAS21, SEBS, and NTSG are the sequence of their  
166 performances. The synthesized ET from PML, SSEBop, MOD16A2105 and NTSG agreed with  
167 the flux EC ET with R-values higher than 0.70, a maximum ME (RME) of 13.94 mm (17.13%)  
168 and a maximum RMSE (RRMSE) of 38.61 mm (47.45%) over 62% of all comparisons levels, as  
169 remotely sensed based ET product spanning from 1982 to 2019 with highest agreements,  
170 accuracies and lower biases over most of the land surface types and conditions. It performs well  
171 when compared with country-based and continental ET products over China, the United States and  
172 the African continent. However, the further synthesis of local ET products is encouraged if  
173 regional ET products are available.”

174

175

176

177

178

179

180

181

182

183

184

185

---

# 186 Synthesis of Global Actual Evapotranspiration from 1982 to 2019

187 Abdelrazek Elnashar<sup>1,2,3</sup>, Linjiang Wang<sup>1,2</sup>, Bingfang Wu<sup>1,2\*</sup>, Weiwei Zhu<sup>1</sup>, Hongwei Zeng<sup>1,2</sup>

188 <sup>1</sup>State Key Laboratory of Remote Sensing Science, Aerospace Information Research Institute, Chinese Academy of  
189 Sciences, Beijing, 100094, China

190 <sup>2</sup>College of Resources and Environment, University of Chinese Academy of Sciences, Beijing, 100049, China

191 <sup>3</sup>Department of Natural Resources, Faculty of African Postgraduate Studies, Cairo University, Giza, 12613, Egypt

192 *Correspondence to:* Bingfang Wu (wubf@aircas.ac.cn)

193 **Abstract.** As a linkage among water, energy, and carbon cycles, global actual evapotranspiration (ET) plays an  
194 essential role in agriculture, water resource management, and climate change. Although it is difficult to estimate ET  
195 over a large scale and for a long time, there are several global ET datasets available with ~~varied uncertainty associated~~  
196 ~~with various assumptions regarding their~~ algorithms, parameters, and inputs, ~~and they produce different levels of~~  
197 ~~uncertainties~~. In this study, we propose a long-term synthesized ET product at a kilometer spatial resolution and  
198 monthly temporal resolution from 1982 to 2019. Through a site-pixel ~~validation~~ evaluation of ~~certain~~ 12 global ET  
199 products over different time periods, land surface types, and conditions, the high performing products were selected  
200 ~~through for synthesis of the new dataset using~~ a high-quality flux eddy covariance covering the entire globe. According  
201 to the study results, Penman-Monteith Leuning (PML), operational Simplified Surface Energy Balance (SSEBop),  
202 Moderate Resolution Imaging Spectroradiometer (MODIS, MOD16A2105) and the Numerical Terradynamic  
203 Simulation Group (NTSG) ET products were chosen to create the synthesized ET set. The proposed product agreed  
204 well with flux EC ET over most of the all comparison levels, with a maximum ME (RME) of 13.94 mm (17.13%) and  
205 a maximum RMSE (RRMSE) of 38.61 mm (47.45%). Furthermore, the product performed better than local ET  
206 products over China, the United States, and the African continent and presented an ET estimation across all land cover  
207 classes. While no product can perform best in all cases, the proposed ET can be used without looking at other datasets  
208 and performing further assessments. Data are available on the Harvard Dataverse public repository through the  
209 following Digital Object Identifier (DOI): <https://doi.org/10.7910/DVN/ZGOUED> (Elnashar et al., 2020) as well as it  
210 is available as Google Earth Engine (GEE) application through this link:  
211 <https://elnashar.users.earthengine.app/view/synthesizedet>.

## 212 1. Introduction

213 Over most of the global land area, terrestrial evapotranspiration (ET) considers the second largest element of  
214 the hydrological cycle after precipitation (Waring and Running, 2007b; Bastiaanssen et al., 2014) and represents the  
215 linkage between water, energy, and carbon cycles (Gentine et al., 2019; Yang et al., 2016; Ferguson and Veizer, 2007)  
216 and ecosystem services (Almusaed, 2011; Yang et al., 2015; Revelli and Porporato, 2018).

217 Hence, the accurate estimation of global ET is essential for understanding the global hydrological cycle and  
218 water budgets (Oki and Kanae, 2006; Trenberth et al., 2007; Rodell et al., 2015), global drought (Sheffield et al.,  
219 2012; Naumann et al., 2018; Spinoni et al., 2019; Lu et al., 2019; Forootan et al., 2019), impacts of climate change  
220 (Waring and Running, 2007a; Zomer et al., 2008; Scheff and Frierson, 2014; Pan et al., 2015), climate change and global

---

221 water resources (Arnell, 1999;Haddeland et al., 2014;Arnell and Lloyd-Hughes, 2014), global transboundary basin  
222 water scarcity (Degefu et al., 2018), water competition within a basin (Scott et al., 2001) and water stress/conflict  
223 within transboundary basins (Samaranayake et al., 2016;Munia et al., 2016;Bastiaanssen et al., 2014).

224 While precipitation and runoff, which are other paramount factors of the global water balance, can be directly  
225 measured by in situ weather stations and stream gauge networks as well as the availability of several datasets of  
226 remotely sensed precipitation (Funk et al., 2015;Ashouri et al., 2015;Huffman et al., 1997;Yamamoto and Shige,  
227 2015), it is difficult to measure ET, especially at large spatial scales (Senay et al., 2012;Zhang et al., 2016).

228 Recently, several global ET datasets have become available for a variety of purposes, and they have been  
229 generated using remote sensing models, land surface models (LSM), and hydrological models (Trambauer et al.,  
230 2014;Li et al., 2018;Sörensson and Ruscica, 2018). There are many differences among these models concerning their  
231 algorithms, parameters, and inputs, and they produce different levels of uncertainty (Wang and Dickinson, 2012;Xu  
232 et al., 2019;Weerasinghe et al., 2020;Vinukollu et al., 2011a). The remote sensing model, which mainly focuses on  
233 thermal remote sensing and the energy balance equation, will be represented by MOD16A2 (Mu et al., 2011), PML  
234 (Zhang et al., 2019), SSEBop (Senay et al., 2013), SEBS (Chen et al., 2013), NTSG (Zhang et al., 2010), and GLEAM  
235 v3.3b (Miralles et al., 2011b). The land surface model uses quantitative methods to simulate the vertical exchanges of  
236 water and energy fluxes between the atmosphere and the land surface, as represented by GLDAS ET (Rodell et al.,  
237 2004), GLEAM v3.3a (Miralles et al., 2011b), and FLDAS (McNally et al., 2017). TerraClimate, which is a  
238 hydrological model, is based on a one-dimensional water balance approach (Abatzoglou et al., 2018). However, the  
239 availability of many datasets introduces challenges related to how users choose the appropriate dataset for their  
240 purposes (Wu et al., 2020).

241 Some studies have evaluated global ET products using an inferred estimate of ET obtained by subtracting  
242 discharge (Q) from precipitation (P),  $ET = P - Q$ , over global river basins (Zhang et al., 2010;Vinukollu et al.,  
243 2011a;Vinukollu et al., 2011b), continental river basins (Weerasinghe et al., 2020), transboundary river basins (Hofste,  
244 2014), and national river basins (Zhong et al., 2020). Some, on the other hand, have used the ensemble ET product as  
245 observed data for evaluating certain ET products (Hofste, 2014;Trambauer et al., 2014;Andam-Akorful et al.,  
246 2015;Bhattarai et al., 2019).

247 ~~Site pixel level validation of certain ET products against flux EC ET as typically observed data has been~~  
248 ~~performed by several studies in specific regions (e.g., globally (Leuning et al., 2008;Zhang et al., 2010;Ershadi et al.,~~  
249 ~~2014;Michel et al., 2016); Asia (Kim et al., 2012); South Africa (Majozi et al., 2017); Europe (Ghilain et al., 2011;Hu~~  
250 ~~et al., 2015); North America (Jiménez et al., 2009;Mu et al., 2011); Europe and the United States (Miralles et al.,~~  
251 ~~2011b); the United States (Vinukollu et al., 2011b;Velpuri et al., 2013;Xu et al., 2019); and China (Jia et al., 2012;Liu~~  
252 ~~et al., 2013;Chen et al., 2014b;Tang et al., 2015;Yang et al., 2017;Li et al., 2018)). Although flux EC ET is commonly~~  
253 ~~flawed, particularly concerning energy balance closure at some sites (Foken, 2008;Helgason and Pomeroy, 2012),~~  
254 ~~relatively short periods, and sparse spatial coverage, it is the most direct method for measuring the exchange between~~  
255 ~~the surface and the atmosphere in different ecosystems (Foken et al., 2012;Baldocchi, 2014). Thus, site-pixel-level~~  
256 ~~validation of certain ET products against flux EC ET as typically observed data has been performed by several studies~~  
257 ~~in specific regions (e.g., globally (Leuning et al., 2008;Zhang et al., 2010;Ershadi et al., 2014;Michel et al., 2016);~~

---

258 [Asia \(Kim et al., 2012\); South Africa \(Majozi et al., 2017\); Europe \(Ghilain et al., 2011;Hu et al., 2015\); North](#)  
259 [America \(Jiménez et al., 2009;Mu et al., 2011\); Europe and the United States \(Miralles et al., 2011b\); the United States](#)  
260 [\(Vinukollu et al., 2011b;Velpuri et al., 2013;Xu et al., 2019\); and China \(Jia et al., 2012;Liu et al., 2013;Chen et al.,](#)  
261 [2014b;Tang et al., 2015;Yang et al., 2017;Li et al., 2018\)\).](#)

262 Few previous studies have focused on merging certain ET products to create an ensemble ET product; for  
263 instance, (Vinukollu et al., 2011a;Mueller et al., 2013;Badgley et al., 2015). They used all ET products and created a  
264 merged product with a low spatial resolution. There are some global merged benchmarking evaporation products.  
265 Vinukollu et al. (2011a) generated an ensemble of six global ET datasets at a daily time scale and  $0.5^{\circ}\times 0.5^{\circ}$  ( $\approx 55$  km)  
266 spatial resolution for the period 1984–2007 using two surface radiation budget products and three models (i.e., surface  
267 energy balance, revised Penman-Monteith, and modified Priestley-Taylor). They reported that the ensemble simple  
268 mean value was reasonable; however, it was generally highly biased globally. Mueller et al. (2013) presented two  
269 monthly global ET products that differed in their input ET members and temporal coverage. The first dataset consisted  
270 of 40 datasets for the period ~~1998–1989~~–1995, while the second dataset merged 14 datasets from 1989 to 2005. Their  
271 ET was derived from satellite and/or in situ observations (diagnostic) or calculated via LSM driven with observation-  
272 based forcing or output from atmospheric reanalysis. Hence, they provided four merged synthesis products, one  
273 including all datasets and three including datasets of each category (i.e., diagnostic, LSM, and reanalysis). They  
274 introduced the first benchmark products for global ET and found that its multi-annual variations showed realistic  
275 responses and were consistent with previous findings. Badgley et al. (2015) used a Priestly-Taylor Jet Propulsion Lab  
276 (PT-JPL) model with 19 different combinations of forcing data to produce global ET estimates from 1984 to 2006 at  
277 a  $1^{\circ}\times 1^{\circ}$  ( $\approx 100$  km) spatial resolution. The ensemble ET members changed according to the number of products  
278 available each year, which ranged between 4 and 12 members for 1999/2000 and 2001/2002, respectively. Their study  
279 focused on the uncertainty in global ET estimates resulting from each class of input forcing datasets.

280 However, from the aforementioned studies, we can report three findings: (1) no single ET product performed  
281 better than any other over different land surface types and conditions, (2) no one generated a single dataset for users,  
282 and (3) the created ensemble ET products relied on several individual ET products and were not based on the product  
283 with the best performance.

284 From our point of view, this work attempts to add to the growing scientific literature using a high-quality  
285 dataset from global flux towers for further validations and inter-comparison between different global ET products to  
286 understand their behavior within defined land cover types, elevation levels, and climatic classes. Moreover, we attempt  
287 to build an ensemble ET product that has a minimum level of uncertainty over as many conditions as possible. The  
288 study has two objectives: (1) to assess global ET products with in situ data derived from global flux towers across a  
289 variety of land surface types and conditions to gain a better understanding of the disparities among datasets and (2) to  
290 synthesize an ensemble global ET product with minimum uncertainties over more land surface types, climate systems,  
291 and monthly, annually and interannual time steps for a longer time.



292 **2. Data**

293 **2.1. Evapotranspiration**

294 Twelve global ET datasets were explored in the current study (Table 1 and Appendix A). Of them, 5 datasets  
 295 used the Moderate Resolution Imaging Spectroradiometer (MODIS) as input, including two versions (V6 and V105)  
 296 of Global Evapotranspiration Project (MOD16A2), Penman-Monteith Leuning ET (PML), the operational Simplified  
 297 Surface Energy Balance ET (SSEBop) and the Surface Energy Balance System (SEBS). One dataset used the  
 298 Advanced Very High-Resolution Radiometer (AVHRR) as input, including the Numerical Terradynamic Simulation  
 299 Group (NTSG). The remainder mainly uses meteorological datasets as direct input, including field measurements such  
 300 as TerraClimate and reanalysis datasets such as FLADS and GLADS. The algorithm used in 12 global ET datasets is  
 301 mainly the Penman-Monteith model, except for FLADS and GLDAS, which use the LSM, and TerraClimate, which  
 302 uses the soil water balance model. Priestley-Taylor is used to estimate evaporation from open water by NTSG while  
 303 Penman evapotranspiration is used in PML for a water body, snow and ice evaporation. SSEBop, SEBS, NTSG, and  
 304 GLEAM are individually managed, and other ET products, as well as elevation data, are available from GEE.

305 **Table 1.** Global ET products.

Product	Method	Satellite data	Meteorological data	Resolution		Temporal coverage
				Spatial	Temporal	
MOD16A2 V6	P-M, SC	MODIS	GMAO	500 m	8 days	Jan 1, 2001 – Ongoing
MOD16A2 V105	P-M, SC	MODIS	GMAO	1 km	8 days	Jan 1, 2000 – Dec 31, 2014
PML	PML	MODIS	GLDAS V21	500 m	8 days	Jul 4, 2002 – Dec 27, 2017
SSEBop	P-M	MODIS	GDAS, PRISM	1 km	1 month	Jan 1, 2003 – Ongoing
SEBS	RS-SEB	MODIS, GLASS, GLAS	ERA-Interim	5 km	1 month	Jan 1, 2001 – Dec 31, 2010
NTSG	Modified P-M & P-T	AVHRR	NCEP/NCAR Reanalysis	8 km	1 month	Jan 1, 1982 – Dec 31, 2013
GLEAM 3.3b	P-T, SSF	Radiation & air temperature	Certain reanalysis data	0.25°	1 month	Jan 1, 2003 – Dec 31, 2018
GLEAM 3.3a	P-T, SSF	-	Certain reanalysis data	0.25°	1 month	Jan 1, 1980 – Dec 31, 2018
FLADS	LSM	MODIS-IGBP, UMD-AVHRR	MERRA-2, CHIRPS	0.10°	1 month	Jan 1, 1982 – Dec 1, 2019
GLDAS V20	LSM	MCD12Q1, MOD44W, GTOPO30	NOAA/GDAS, GPCP, AGRMET	0.25°	3 hours	Jan 1, 1948 – Dec 31, 2010
GLDAS V21	LSM	MCD12Q1, MOD44W, GTOPO30	NOAA/GDAS, GPCP, AGRMET	0.25°	3 hours	Jan 1, 2000 – Dec 23, 2019
TerraClimate	SWB	Root zone storage capacity	WorldClim V1.4&2, CRU Ts4.0, JRA-55	0.25°	1 month	Jan 1, 1958 – Dec 1, 2018

306 Note: P-M: Penman-Monteith; PML: P-M Leuning; SC: Surface Conductance; P-T: Priestley-Taylor; RS-SEB: remotely sensed  
 307 surface energy balance; LSM: land surface model; SWB: soil water balance; GMAO: Global Modelling and Assimilation Office  
 308 for daily meteorological reanalysis data; GDAS: Global Data Assimilation System; PRISM: Parameter-elevation Regressions on  
 309 Independent Slopes Model; GLASS: Global Land Surface Satellite; GLAS: Geoscience Laser Altimeter System; MERRA-2:  
 310 Modern-Era Retrospective analysis for Research and Applications version 2; CHIRPS: Climate Hazards Group InfraRed  
 311 Precipitation with Station data; RFE2: The African Rainfall Estimation version 2.0; NOAA: National Oceanic and Atmospheric  
 312 Administration; GPCP: Global Precipitation Climatology Project; AGRMET: Agricultural Meteorological modeling system; CRU  
 313 Ts4.0: Climate Research Unit time series data version 4.0; JRA-55: Japanese 55-year Reanalysis.

314 Three regional ET datasets were used for comparison of consistent agreement over China, the United States  
315 and the African continent (Table 2). Over China Mainland, The Complementary Relationship (CR) ET product was  
316 used (Ma et al., 2019); it is estimated monthly at a 0.1° (≈10 km) spatial resolution over 1982–2015 and can be  
317 retrieved from <http://en.tpdatabase.cn/>. For the United States, daily SSEBop was used (Savoca et al., 2013; Senay and  
318 Kagone, 2019). These data are produced at a 0.009°×0.009° (≈1 km) grid cell spatial resolution from 2000 to 2018  
319 and can be downloaded from <https://earlywarning.usgs.gov/ssebop/modis/daily/>. Daily SSEBop aggregated to  
320 monthly time steps to be comparable with the synthesized ET temporal resolution. The Food and Agriculture  
321 Organization (FAO) Water Productivity through Open access of Remotely sensed derived ET product (FAO WaPOR  
322 version 2) was used for Africa (FAO, 2018, 2020). These data estimates are the sum of ET and interception, provided  
323 at a 0.002°×0.002° (≈250 m) spatial resolution with a monthly temporal resolution from 2009. WaPOR ET estimates  
324 are available through the following website: [https://wapor.apps.fao.org/home/WAPOR\\_2/1/](https://wapor.apps.fao.org/home/WAPOR_2/1/).

325 **Table 2.** Regional ET products.

Product	Method	Satellite data	Meteorological data	Resolution		Temporal coverage
				Spatial	Temporal	
CR	CR	MODIS	CMFD	10 km	1 month	Jan 1, 1982 – Dec 31, 2015
SSEBop	P-M	MODIS	NASA GDAS	1 km	1 day	Jan 1, 2000 – Dec 31, 2018
WaPOR	RS-SEB	MODIS	MERRA/GEOS-5, CHIRPS	250 m	1 month	Jan 1, 2009 – Ongoing

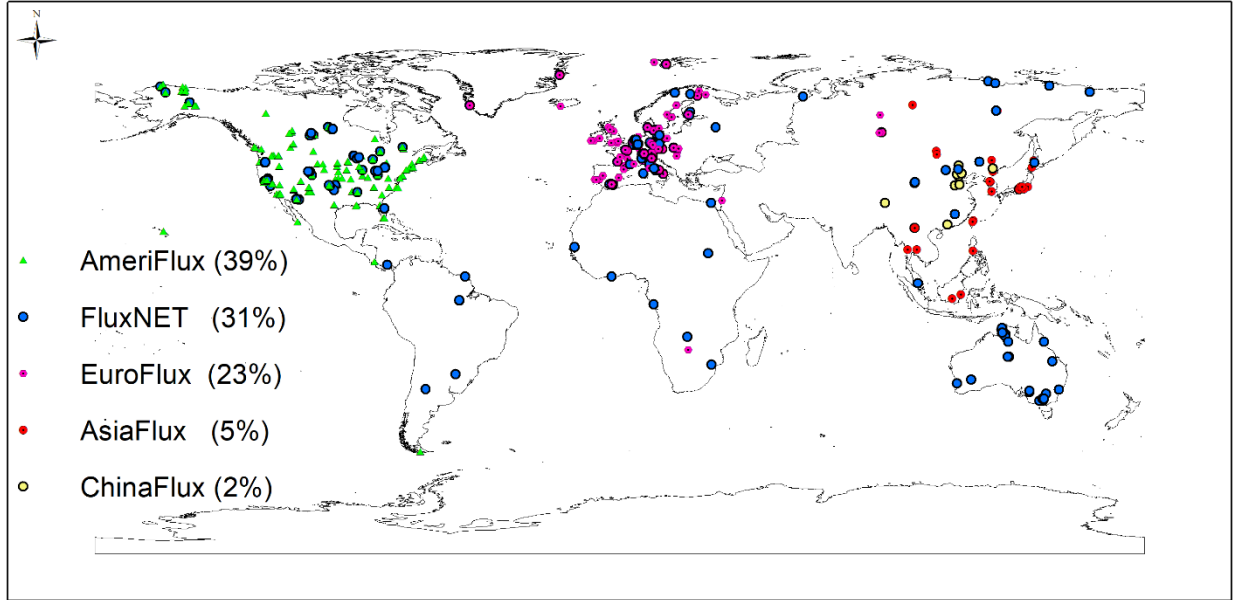
326 Note: CR: Complementary Relationship; P-M: Penman-Monteith; P-T: Priestley-Taylor; RS-SEB: remotely sensed surface energy  
327 balance; CMFD: China Meteorological Forcing Dataset; NASA GDAS: National Oceanic and Atmospheric Administration's  
328 (NOAA) Global Data Assimilation System; MERRA: Modern-Era Retrospective Analysis for Research and Applications; GEOS-  
329 5: Goddard Earth Observing System, Version 5; CHIRPS: Climate Hazards Group InfraRed Precipitation with Stations.

## 330 2.2. Flux EC data

331 Comprehensive flux EC ET data from 645 sites (Fig. 1 and Table 3), AmeriFlux; FluxNET; EuroFlux;  
332 AsiaFlux; and ChinaFlux, were collected and processed to examine the performance of different estimated ET  
333 products. The downloaded EC data are half-hourly text-type data, while the periods of flux EC ET ranged from 1 year  
334 (12 months) to 21 years (252 months) from 1994 to 2019. The gap-filling technique was applied to the downloaded  
335 in situ EC data (Reichstein et al., 2005). Different EC flux sites were spatially distributed on the heterogeneous  
336 underlying surface, corresponding to different land cover types according to the International Geosphere-Biosphere  
337 Programme (IGBP) classification system, which is recorded in each flux attribute data. The in-situ measured ET (mm  
338 day<sup>-1</sup>) can be obtained by the half-hourly average latent heat flux ( $\overline{LE}$ ,  $W \cdot m^{-2} \cdot s^{-1}$ ) through Eq. (1), (Su, 2002):

$$ET = \frac{\overline{LE}}{\lambda} \times 3600 \times 24 \quad (1)$$

339 Where  $\overline{LE}$  ( $W \cdot m^{-2} \cdot s^{-1}$ ) is the daily average of the half-hourly average latent heat flux, and  $\lambda$  is the latent heat of  
340 evaporation.  $\lambda$  varies with air temperature in hydrologic or agricultural system modeling but only to a small extent  
341 (Walter et al., 2001), and the value acts directly on the accuracy of the estimated in situ measured ET. Considering  
342 that there are very limited impacts of the changes in air temperature on the estimated in-situ measured ET (Henderson-  
343 Sellers, 1984; Li et al., 2018), the constant value of 2.45 MJ kg<sup>-1</sup> is fixed in the calculation above (Walter et al., 2001).



344  
345 **Figure 1.** Spatial distribution of 645 in-situ flux EC sites across the world.

346 **Table 3.** Summary of 645 in-situ EC flux sites.

Flux	Sites number	Temporal coverage	Elevation range (m)	Underlying surface IGBP type	Website
AmeriFlux	249	1994–2019	-9 to 3199	ENF/EBF/DBF/MF/CSH/OSH/WSA/SAV/SA/SAV/GRA/WET/CRO	ameriflux.lbl.gov
FluxNET	203	1994–2019	-10 to 4312	ENF/EBF/DBF/MF/CSH/OSH/WSA/SAV/SA/SAV/GRA/WET/CRO	fluxnet.fluxdata
EourFlux	148	1996–2018	-4 to 2436	ENF/EBF/DBF/MF/CSH/OSH/WSA/SAV/SA/SAV/GRA/WET/CRO	europe-fluxdata.eu
AsiaFlux	33	2000–2015	0 to 3308	ENF/EBF/DBF/MF/CSH/OSH/WSA/SAV/SA/SAV/GRA/WET/CRO/URB/WAT	asiaflux.net
ChinaFlux	12	2003–2017	26 to 4317	EBF/MF/GRA/CRO	chinaflux.org

347 Note: ENF: Evergreen Needleleaf Forests; EBF: Evergreen Broadleaf Forests; DBF: Deciduous Broadleaf Forests; MF: Mixed  
348 Forests; CSH: Closed Shrublands; OSH: Open Shrublands; WSA: Woody Savannas; SAV: Savannas; GRA: Grasslands; WET:  
349 Permanent Wetlands; CRO: Croplands; URB: Urban and Build-up Lands; SNO: Permanent Snow and Ice; BSV: Barren or Sparsely  
350 Vegetated Area; WAT: Water Bodies.

### 351 2.3. Aridity index

352 The mean global aridity index dataset was produced by (Zomer et al., 2008) using WorldClim global climate  
353 data. The aridity index was estimated as the mean annual precipitation divided by the mean annual potential  
354 evapotranspiration, and the latter was calculated by the Hargreaves equation. The spatial resolution was  
355  $0.0083^{\circ} \times 0.0083^{\circ}$  ( $\approx 1$  km) grid cell (Trabucco and Zomer, 2018) and the data can be downloaded from the following  
356 website: <https://cgiarcsi.community/data/global-aridity-and-pet-database/>

### 357 2.4. Elevation data

358 The Shuttle Radar Topography Mission (SRTM) data were provided at a resolution of one arc-second and  
359 void-filled (Farr et al., 2007). For the geographic areas outside the SRTM coverage area, the Global Multi-resolution  
360 Terrain Elevation Data 2010 (GMTED2010), which have a resolution of 7.5 arc-seconds, were used (Danielson and  
361 Gesch, 2011).

### 362 3. Methods

#### 363 3.1 Assessment

364 Because ET is highly variable in both space and time (Schaffrath and Bernhofer, 2013;Fisher et al., 2017), a  
365 comprehensive evaluation from different perspectives is required (Trambauer et al., 2014;McCabe et al., 2016;Li et  
366 al., 2018). For each flux tower location, the aridity index, elevation and estimated ET data were extracted. The aridity  
367 index was classified (Table 4) according to the United Nations Environment Programme definition (UNEP, 1997) into  
368 four classes (i.e., humid: 361 (56%), semiarid: 167 (26%), dry sub-humid: 82 (13%), and arid: 35 (5%)). Elevations  
369 were classified into three levels (i.e., <500 m: 452 (70%), 500 m–1500 m: 135 (21%), and >1500 m: 58 (9%)). Land  
370 cover included five types (i.e., forests: 349 (54%), grasslands: 128 (20%), croplands: 89 (14%), water bodies: 73  
371 (11%), and others (barren land and permanent snow and ice): 6 (1%)). Accordingly, the following metrics were  
372 estimated using Eqs. (2-7):

$$373 \text{ ME} = \frac{1}{n} \sum_{i=1}^n Y_i - X_i \quad (2)$$

$$374 \text{ RME} = \frac{\text{ME}}{\bar{X}} \quad (3)$$

$$375 \text{ RMSE} = \sqrt{\frac{\sum_{i=1}^n (Y_i - X_i)^2}{n}} \quad (4)$$

$$376 \text{ RRMSE} = \frac{\text{RMSE}}{\bar{X}} \quad (5)$$

$$377 \text{ R} = \frac{\sum_{i=1}^n [(Y_i - \bar{Y})(X_i - \bar{X})]}{\sqrt{\sum_{i=1}^n (Y_i - \bar{Y})^2} \sqrt{\sum_{i=1}^n (X_i - \bar{X})^2}} \quad (6)$$

$$378 \text{ TS} = \frac{4(1 + \text{R})}{\left(\text{std} + \frac{1}{\text{std}}\right)^2 (1 + \text{R}_0)} \quad (7)$$

373 Where ME is the mean error; RME is the relative mean error; RMSE is the root mean square error; RRMSE is the  
374 relative root mean square error; R is the correlation coefficient; TS is the Taylor score; n is the sample number; i is  
375 the  $i^{\text{th}}$  sample; X is the mean of the observed EC ET data; Y is the mean of different estimated ET data; std is the  
376 standard deviation of the estimated ET normalized by the standard deviation of the observed EC ET; and  $R_0$  is the  
377 maximum theoretical R, with an  $R_0$  value of 0.9976 (Taylor, 2001).

378 The magnitude of ME (the absolute value) is used as a bias indicator (Mu et al., 2011;Yang et al., 2017),  
379 while its sign indicates whether different ET products overestimate or underestimate the flux EC ET values. The  
380 accuracy of each ET product can be described by the RMSE (Miralles et al., 2011b;Hu et al., 2015). Moreover, the  
381 relative values of ME and RMSE are used for a fairer comparison between certain ET products among different regions  
382 and periods (Majozi et al., 2017). In addition, correlation coefficients (R values) are used to measure the strength of  
383 the relation between flux EC ET and different ET products (Ghilain et al., 2011;Hu et al., 2015), and with the aid of  
384 the Taylor score (TS), the overall performance of each product can be described well (Taylor, 2001;Mu et al., 2011).  
385 To rank each ET product, the lower ME, RME, RMSE, and RRMSE values and the higher R and TS values are desired;  
386 lower biases and higher accuracies.

387

388 **Table 4.** Climate classification according to the global aridity index values.

Aridity Index value	Climate class
<0.03	Hyper arid
0.03 – 0.20	Arid
0.20 – 0.50	semiarid
0.50 – 0.65	Dry sub-humid
>0.65	Humid

389 **3.2 Synthesis method**

390 There are 6 validation metrics including R, TS, ME, RME, RMSE, and RRMSE. The validation values of 6  
 391 metrics are categorized into levels. The level one of validation metrics has the highest R and TS values and the lowest  
 392 ME, RME, RMSE, and RRMSE while the level two of validation metrics has the highest R and TS values and the  
 393 lowest ME, RME, RMSE, and RRMSE after level one. For that, R and TS sorted descending while ME, RME, RMSE,  
 394 and RRMSE sorted ascending (Fig. 2a) then the corresponding ET product of each validation metric saved in a new  
 395 table to be used to fill in Fig. 2b.

396 The current study proposes three steps to develop a synthesized global ET dataset. First, the ET datasets are  
 397 compared based on 6 validated metrics, in which to generate a matrix ~~was developed~~ to indicate level one and two of  
 398 the validation metrics of all ET products over all comparison levels, see Table 5. There (Fig. 2b). For each level, there  
 399 are six validation criteriametrics in rows (i.e., ME (mm), RME (%), RMSE (mm), RRMSE (%), R, and TS) and 26  
 400 ET values of different periods and 26 underlying conditions in columns (comparison levels in columns (i.e.), including  
 401 monthly average (01), annual average (02), monthly (January-December: 03–14), land cover types (15–19), climate  
 402 classes (20–23), and elevation levels (24–26)). The). Thus, the total number of cells is 156; for each level. Each cell  
 403 in the matrix represents a free competition between certain one of twelve ET products that belong to occupy this cell  
 404 based on each validation criterion level. Then, selecting to select ET data for further synthesis, based on the magnitudes  
 405 (absolute values) of each validation index of all ET products across all comparison classes (01–26), the best first the  
 406 number and second levels of ET products within each cell were selected; additionally, the count and percent of each  
 407 percentage of ET product in all cells occurrence at matrix (Fig. 2b) of level one and two were calculated to calculate  
 408 the total count and percent from levels one and two, see Table 6. All (Fig. 2c). ET products will be sorted were ranked  
 409 in descending order based on the total occurrence percentage of levels one and two. (the last column in Fig. 2c). Finally,  
 410 the first two or three highly ranked ET products were incorporated selected to incorporate into the ensemble ET. For  
 411 that, the selected ET products were resampled to a comparable spatial resolution if needed, and the average was used  
 412 as the synthesized ET value.

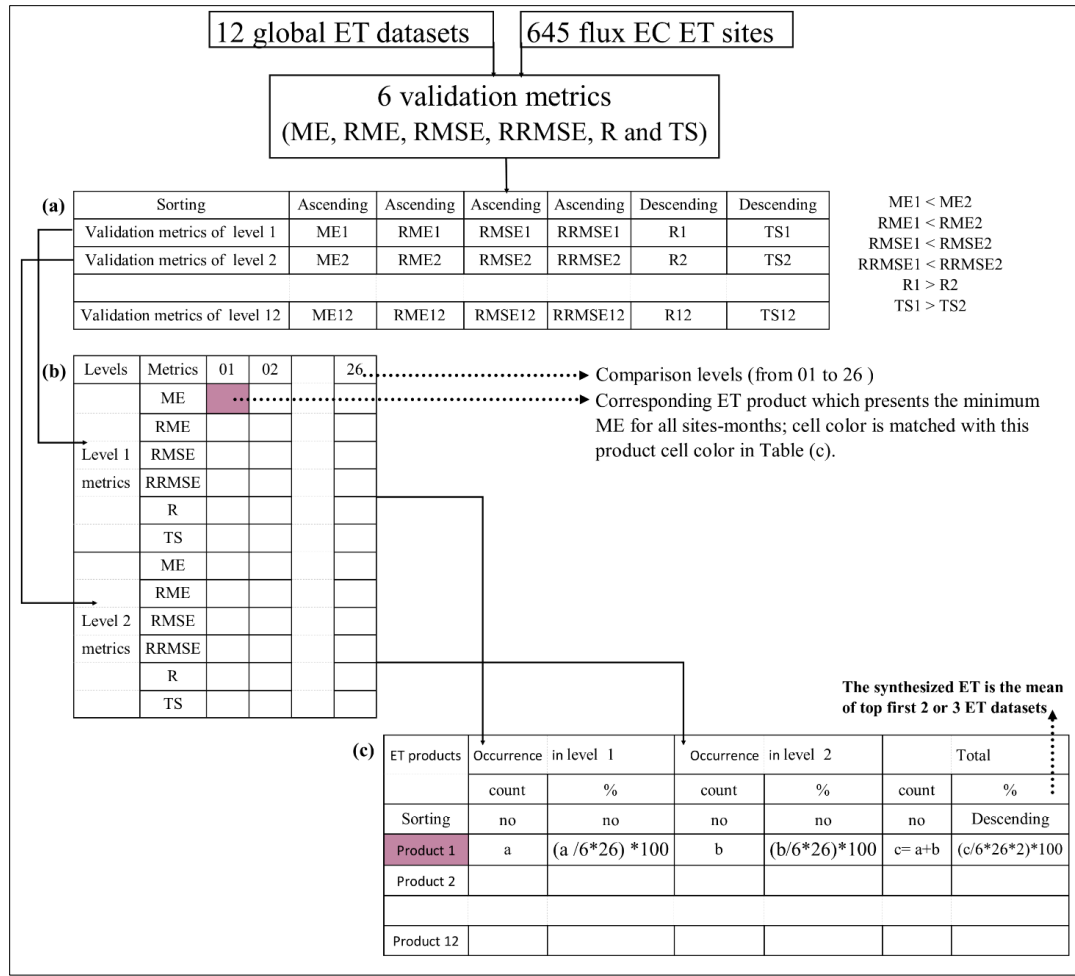


**Figure 2. Flowchart of the synthesis method.**

413

414

## 415 4. Results

### 416 4.1. Assessment of existing global ET datasets

417 Figure 23 shows that seasonality exists and is captured well by all ET datasets, with some exceptions over  
 418 barren land, permanent snow and ice, and arid areas (not shown). The maximum ET occurs during July and differs  
 419 according to each ET dataset. Generally, MOD16A2 represents the minimum estimated ET across all conditions, while  
 420 SSEBop represents the maximum ET across all conditions except over humid regions and at elevations between 500  
 421 m and 1500 m. From Figures (3, 5-114, 6-12), the best-fitted linear regression line (blue-solid line) compared to the  
 422 1:1 line (red-dashed line), all ET datasets overestimate the flux EC ET in lower ET values and underestimate the flux  
 423 EC ET in higher ET values with two exceptions. The first exception is over barren land and permanent snow and ice,  
 424 where MOD16A2 underestimates and GLDAS21, GLEAM33a, and TerraClimate overestimate under both lower and  
 425 higher ET values (not shown). Second, in dry sub-humid areas, SSEBop (Fig. 9c3) and GLDAS21 (Fig. 9e3)  
 426 overestimate under both lower and higher ET values. Applying for the highest R (TS) and lowest error metrics role,

---

427 MOD16A2 cannot present any role; additionally, only one contribution by the lowest RRMSE was found in February  
428 and the highest TS was found in March for TerraClimate and GLEAM33b, respectively.

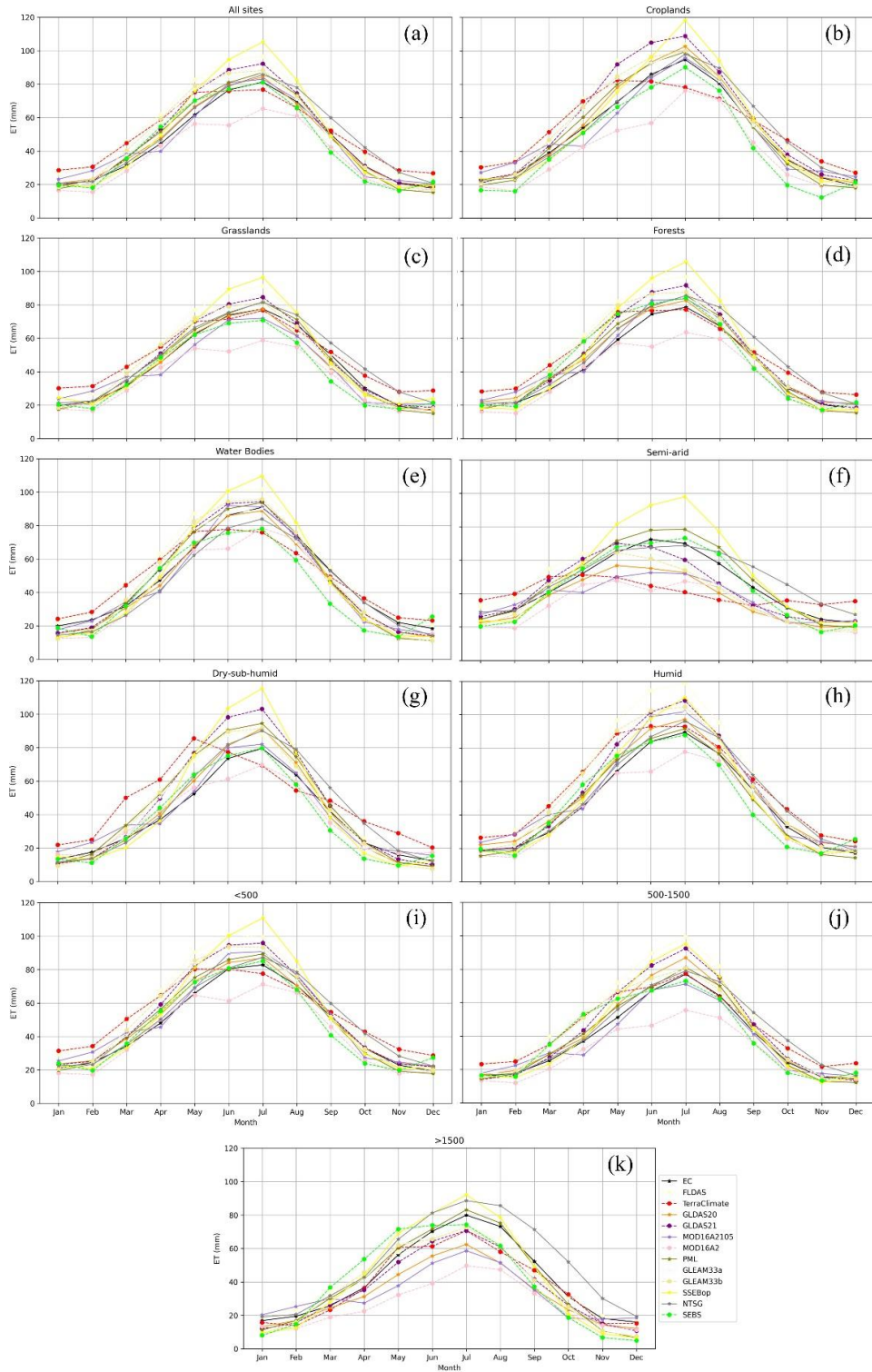
#### 429 4.1.2. Validation by all sites' monthly ET

430 Figure 34 shows that only SEBS and MOD16A2 underestimate flux EC ET. PML is the dataset that best  
431 agrees with the observed ET, and it had the lowest RMSE (RRMSE). MOD16A2105 returned the smallest absolute  
432 ME, while SEBS yielded the smallest RME. Figure 45 shows there are interannual differences between certain ET  
433 product performances. MOD16A2 shows negative MEs and RMEs for all months, with larger biases during March,  
434 April, and May, while FLDAS shows positive MEs and RMEs for all months, with larger biases during March, April  
435 May, June, and July. For other products, the ME and RME signs vary among months; for instance, the ME and RME  
436 values of GLDAS21 are negative (underestimated) during February, September, and November and positive  
437 (overestimated) in the remaining months, with larger biases during March, April, May, June, and July. The RMSE  
438 declines from January to February and then increases until July and declines again until November. The minimum  
439 RMSE values occur during February, November, and December, while the maximum values occur during June, July,  
440 and August.

441 For instance, the RMSE in July ranges from 36.28 mm to 52.41 mm for FLDAS and PML, respectively,  
442 while it ranges from 17.08 mm to 21.68 mm for PML and SEBS, respectively. RRMSE declines from January reaches  
443 its minimum in June and then increases again until December, except for SEBS in December. The highest values of  
444 RRMSE (>80%) occur in January, February, November, and December except for SEBS in December, while the  
445 lowest values (<60%) exist in June, July, and August. The R-value declines from January and reaches its minimum in  
446 May; it then increases starting in August. Except for MOD16A2, all products have an R-value greater than 0.60 during  
447 January, February, November, and December. SEBS has the lowest R-value during March, April, May, and June,  
448 while PML yields the highest R-value during all months except January and December. Except for MOD16A2 in  
449 February, which has a TS value above 0.60, as with the R-value, the TS declines from January, reaches its minimum  
450 in May, and then increases again starting in August. Figures 3 and 4 and 5 show these products yield intra-annual ET  
451 variations but vary in their performance according to the selected validation metrics, which also vary among all months  
452 (from January to December).

453

454



455  
456  
457  
458

**Figure 23.** Monthly average flux EC ET and 12 ET products over all flux sites (a), land cover types (croplands: (b); grasslands: (c); forests: (d); water bodies: (e)), climate classes (semiarid: (f); dry sub-humid: (g); humid: (h)), and elevation levels (<500 m: (i), 500 m-1500 m: (j), and >1500m: (k)).

459



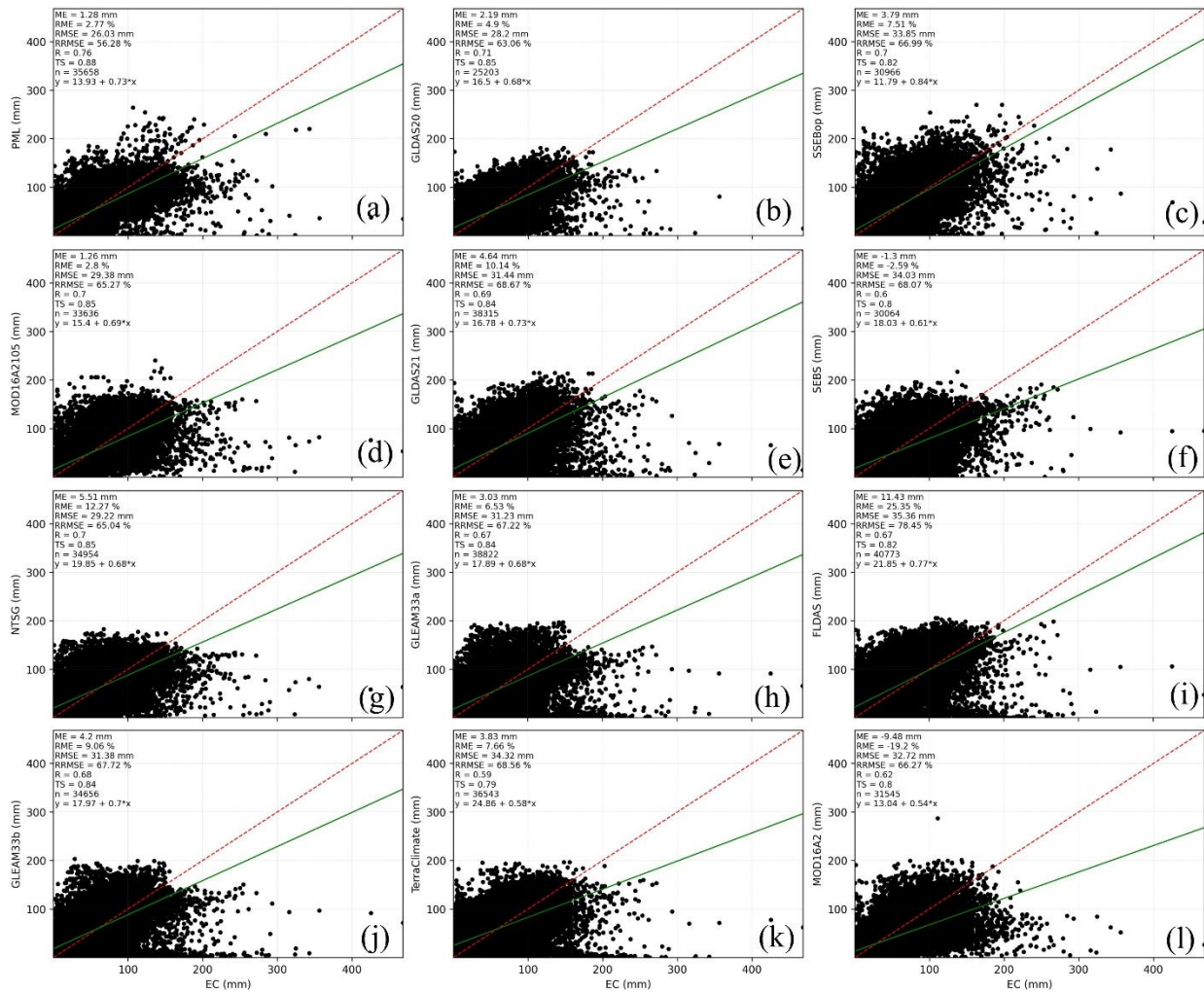


**Figure 34.** Monthly ET products (PML: (a); GLDAS20: (b); SSEBop: (c); MOD16A2105: (d); GLDAS21: (e); SEBS: (f); NTSG: (g); GLEAM33a: (h); FLDAS: (i); GLEAM33b: (j); TerraClimate: (k); MOD16A2: (l)) against flux EC ET aggregated for all sites.

460  
461  
462

463

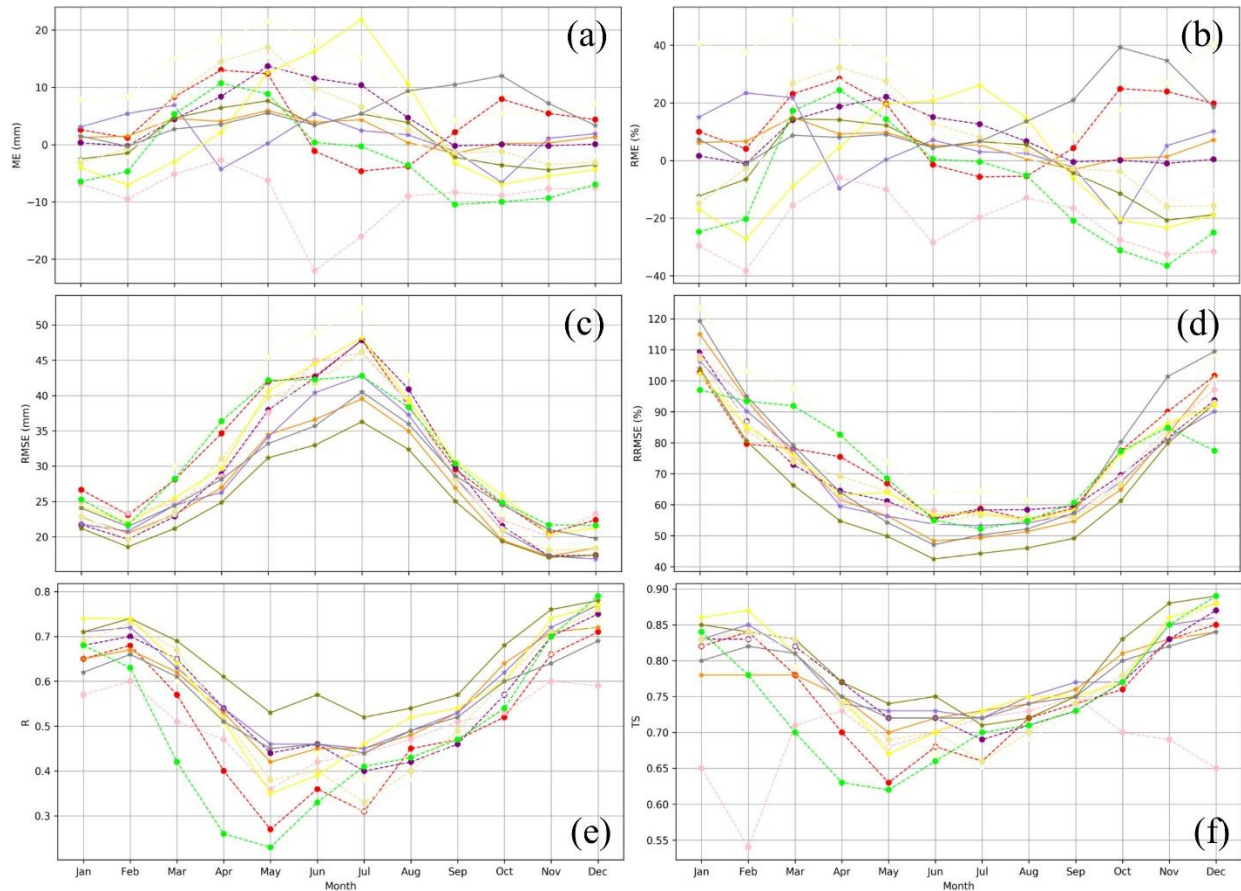


**Figure 45.** Monthly validation metrics (ME (mm): (a); RME (%): (b); RMSE (mm): (c); RRMSE (%): (d); R: (e); TS: (f)) of ET products against flux EC ET for all sites (legend as Figure 243k).

#### 4.1.3. Validation by all sites' annual ET

Figure 56 shows all ET products overestimate the observed ET with two exceptions; SEBS and MOD16A2. In all environmental conditions, PML has the highest R (TS) and the lowest ME (RME) and RMSE (RRMSE). Figures 34 and 56 indicate the obvious error metrics of annual scale performances that are consistent with those that come from the monthly time step. The lowest and highest absolute values of ME (RME) for monthly ET exist in MOD16A2105 (SEBS) and FLDAS, respectively, while those for annual ET exist in PML and FLDAS, respectively. Furthermore, PML yields the largest R and TS values for monthly and annual ET, but the minimum values of R and TS were registered with TerraClimate and MOD16A2 for monthly and annual ET, respectively. This result may be attributed to the aggregation of monthly ET into annual values.

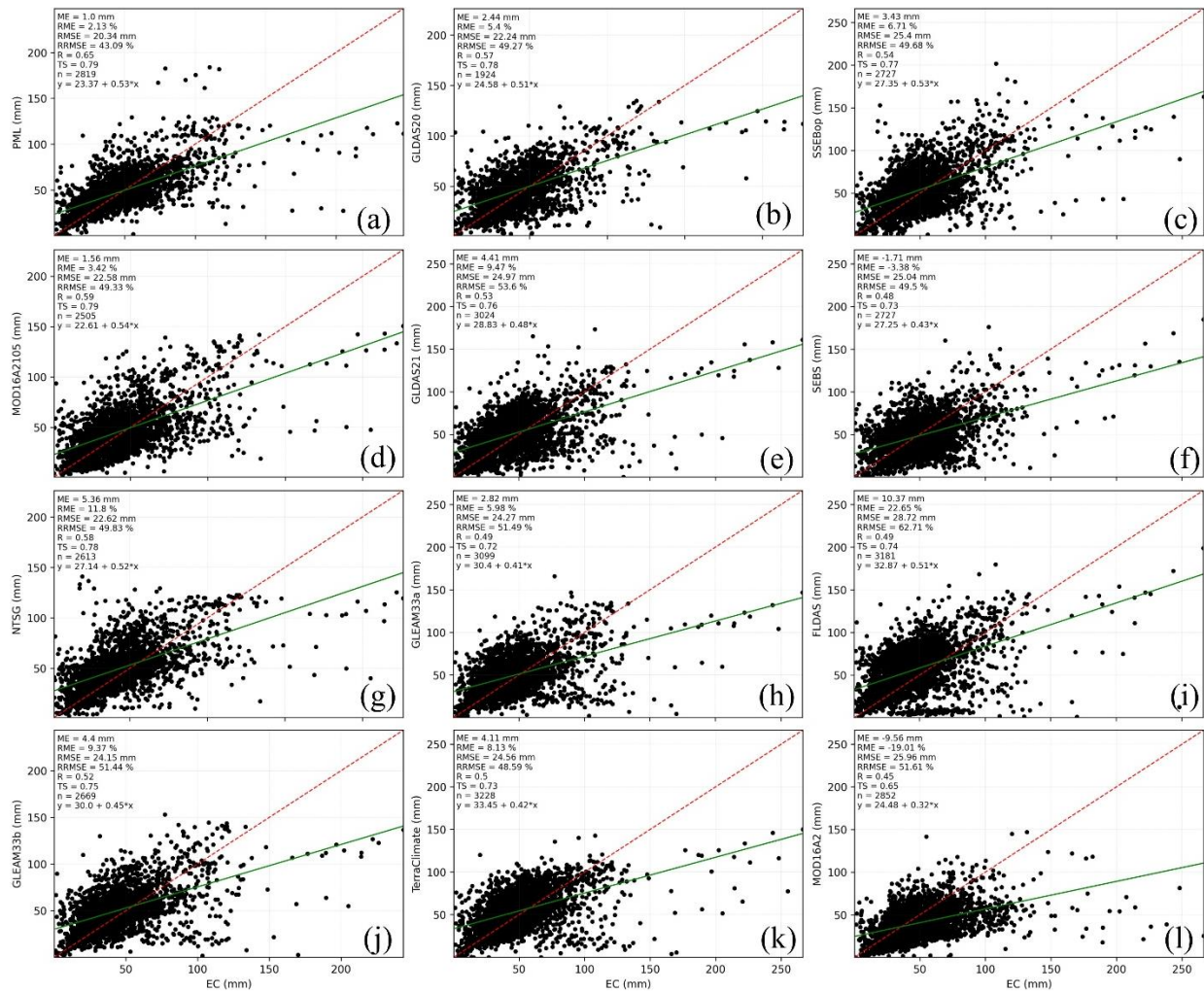
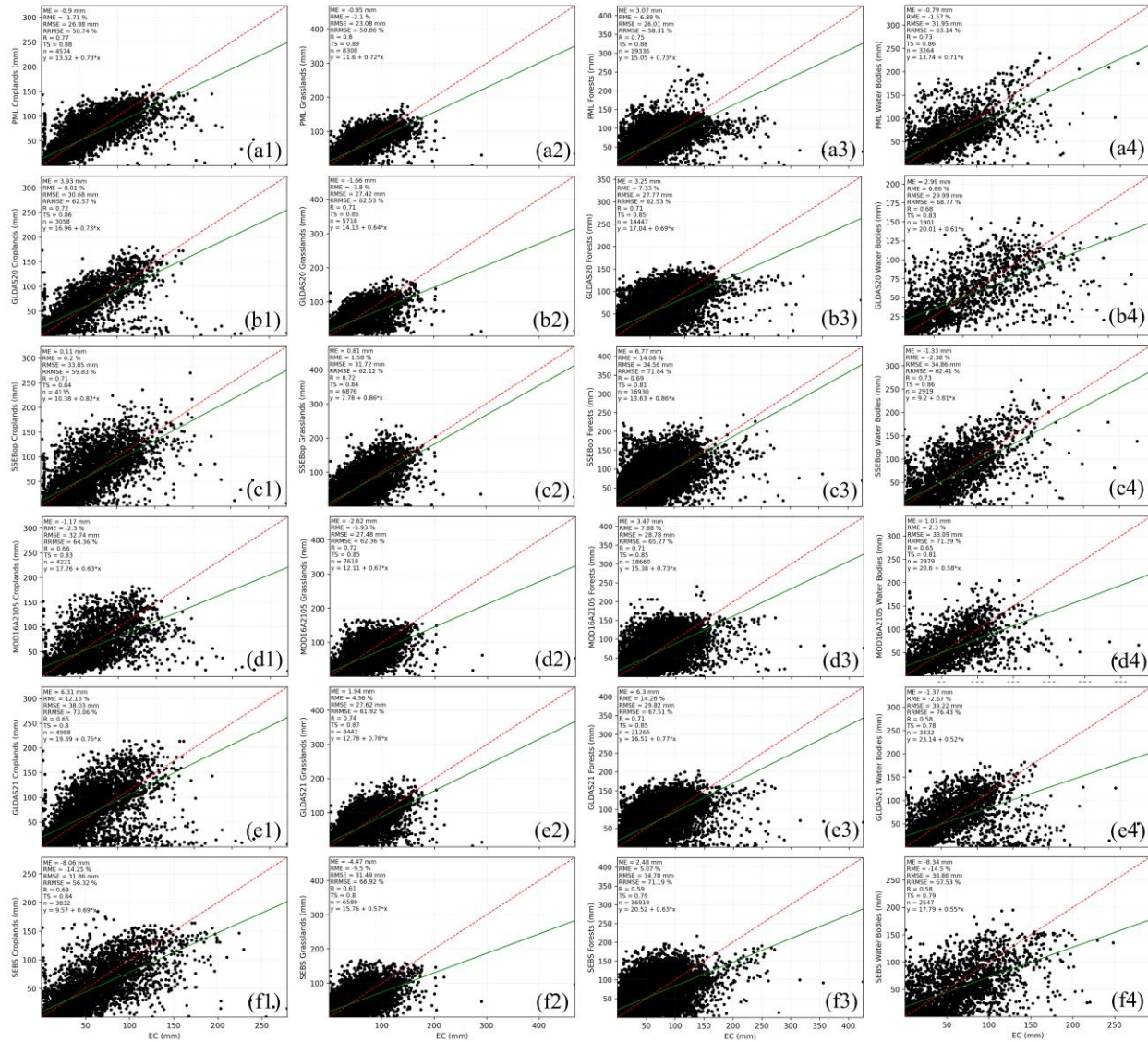


**Figure 56.** Annually ET products (PML: (a); GLDAS20: (b); SSEBop: (c); MOD16A2105: (d); GLDAS21: (e); SEBS: (f); NTSG: (g); GLEAM33a: (h); FLDAS: (i); GLEAM33b: (j); TerraClimate: (k); MOD16A2: (l)) against flux EC ET aggregated for all sites. (subplot label as in Figure 4).

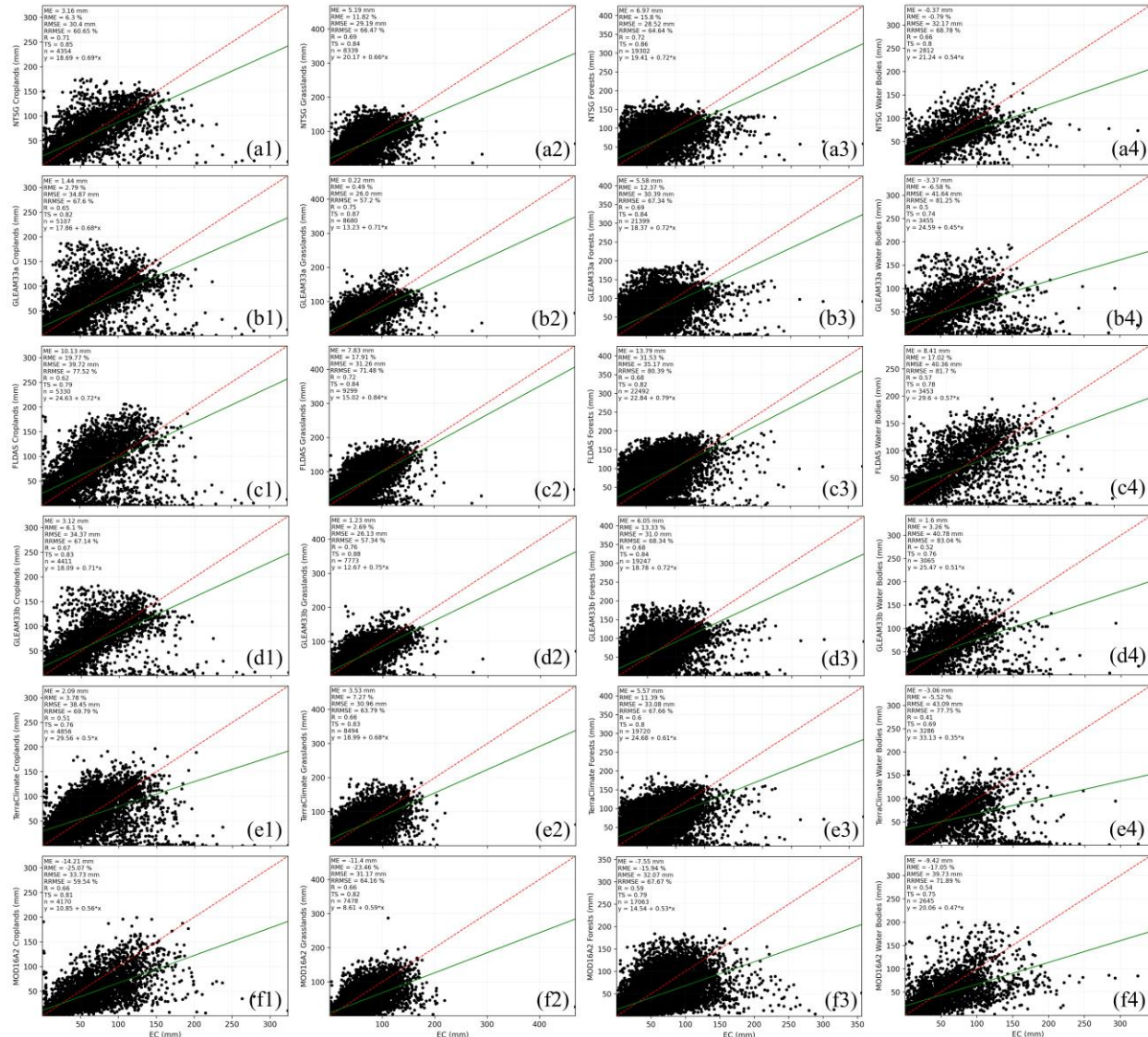
#### 4.1.4. Validation by land cover types

Figures 67 and 78 show that, according to the ME (RME) sign, except for some ET products over croplands (i.e., MOD16A2, SEBS, MOD16A2105, and PML), grasslands (i.e., MOD16A2, SEBS, MOD16A2105, GLDAS20, and PML), forests (MOD16A2), and barren land and permanent snow and ice (i.e., MOD16A2105, MOD16A2, FLDAS, and GLDAS20), which underestimate the flux EC ET, the other ET products overestimate. For water bodies, MOD16A2105, GLEAM33b, GLDAS20, and FLDAS overestimate, while the other products produce underestimates. Over croplands, grasslands, and forests, PML is the best product for R (TS) and RMSE (RRMSE). Additionally, it has the highest TS over water bodies. SSEBop, GLEAM33a, SEBS, NTSG, and GLDAS20 obtained the desired ME (RME) over croplands, grasslands, forests, water bodies, and barren land and permanent snow and ice, respectively. GLEAM33a also represents the highest R (TS) with the lowest RRMSE, while GLDAS20 has the smallest RMSE over barren land and permanent snow and ice. In addition, GLDAS20 has the lowest RMSE, while SSEBop has the highest R and lowest RRMSE over water bodies, see Table 5 (level one: 15–19).



494  
 495 **Figure 67.** Monthly ET products (PML: (a); GLDAS20: (b); SSEBop: (c); MOD16A2105: (d); GLDAS21: (e); SEBS: (f)) against  
 496 flux EC ET aggregated for all sites for each land cover type (croplands: (1); grasslands: (2); frosts: (3); water bodies: (4)).

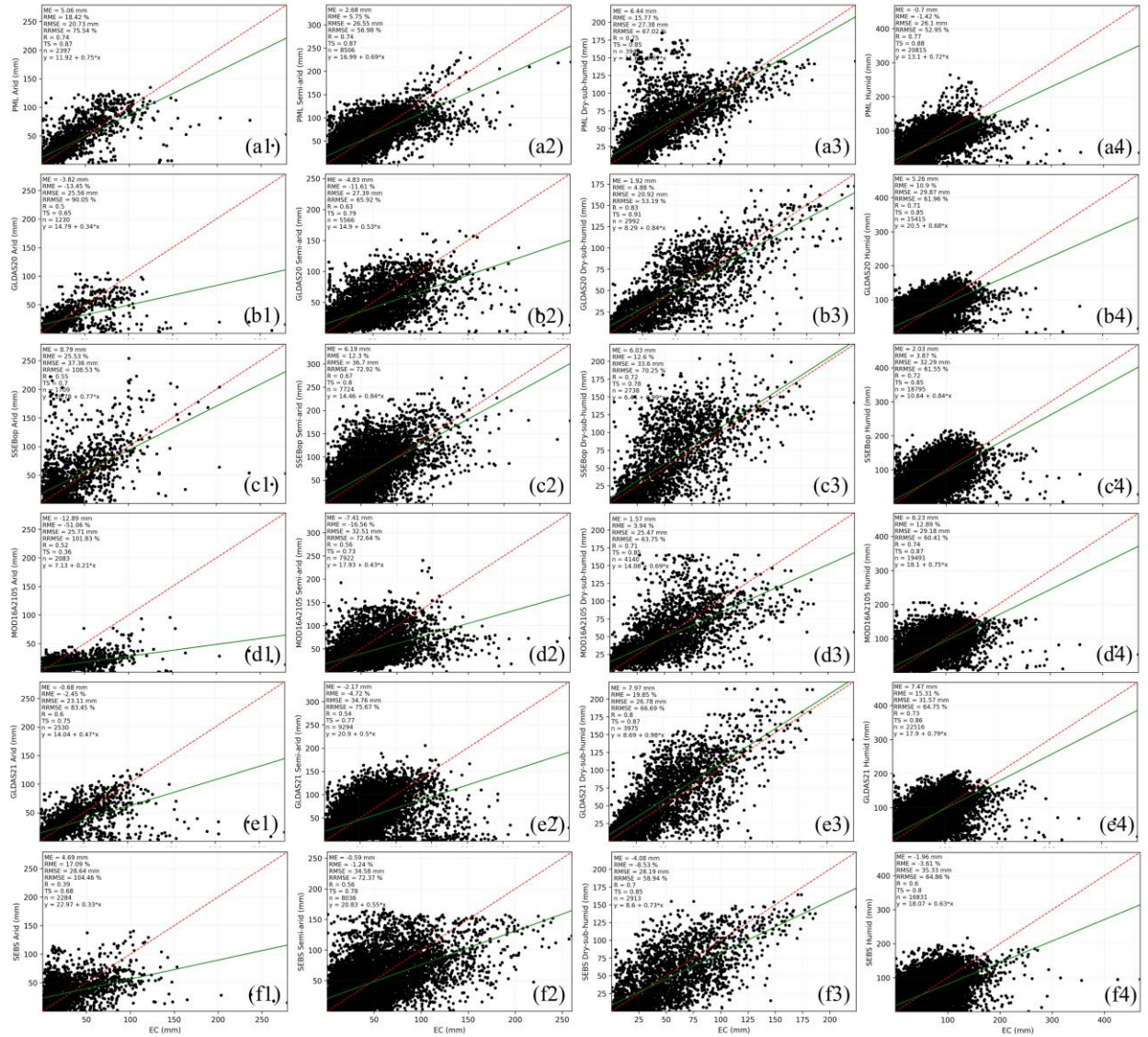
497  
 498  
 499  
 500  
 501  
 502  
 503



504  
 505 **Figure 78.** Monthly ET products (NTSG: (a); GLEAM33a: (b); FLDAS: (c); GLEAM33b: (d); TerraClimate: (e); MOD16A2: (f))  
 506 against flux EC ET aggregated for all sites for each land cover type (croplands: (1); grasslands: (2); forests: (3); water bodies: (4)).

507 **4.1.5. Validation by climate classes**

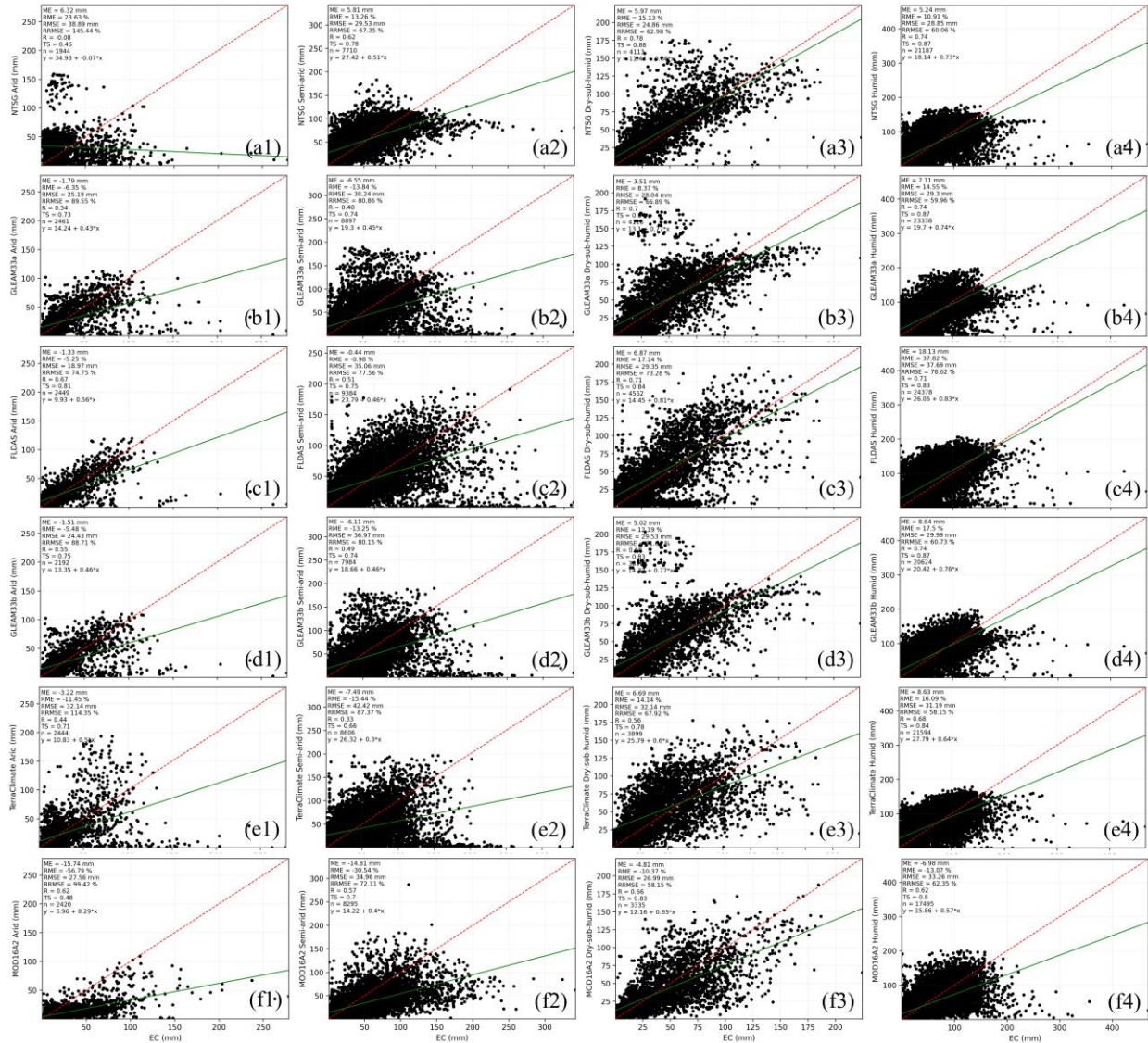
508 Figures 89 and 910 show that SEBS, PML, NTSG, and SSEBop in arid areas and PML, NTSG, and SSEBop  
 509 in semiarid areas overestimate values, while MOD16A2 and SEBS in dry sub-humid areas and MOD16A2, SEBS,  
 510 and PML in humid areas underestimate values; for each aridity index class, other products were the opposite. Over  
 511 humid areas, PML represents the highest agreement and accurate dataset compared to the flux EC ET. Furthermore,  
 512 it had the highest R (TS) in the arid and semiarid areas and the smallest RMSE (RRMSE) in semiarid areas. GLDAS20  
 513 yielded the largest R (TS) with the smallest RMSE (RRMSE) in dry-sub-humid regions; over these regions,  
 514 MOD16A2105 presented the best ME (RME). FLDAS has two contributions, with the smallest ME (RME) and RMSE  
 515 (RRMSE) in semiarid and arid areas, respectively, while GLDAS21 has only one point over arid areas where the best  
 516 ME (RME) is found, see Table 5 (level one: 20–23).



517  
518  
519

**Figure 89.** Monthly ET products (PML: (a); GLDAS20: (b); SSEBop: (c); MOD16A2105: (d); GLDAS21: (e); SEBS: (f)) against flux EC ET aggregated for all sites for each climate class (arid: (1); semiarid: (2); dry-sub-humid: (3); humid: (4)).

520  
521  
522  
523  
524  
525  
526  
527  
528  
529



530  
531 **Figure 910.** Monthly ET products (NTSG: (a); GLEAM33a: (b); FLDAS: (c); GLEAM33b: (d); TerraClimate: (e); MOD16A2:  
532 (f)) against flux EC ET aggregated for all sites for each climate class (arid: (1); semiarid: (2); dry-sub-humid: (3); humid: (4)).

533 **4.1.6. Validation by elevation levels**

534 Figures 4011 and 412 show that MOD16A2 and SEBS over elevation levels <500 and MOD16A2 and  
535 MOD16A2105 over elevation levels from 500 m to 1500 underestimate the values, while the other ET products  
536 overestimate the values; additionally, at elevations >1500, only SSEBop and NTSG overestimate the values. The ET  
537 product agreed best with the desired RMSE (RRMSE) in the PML product. Moreover, it yielded the best ME (RME)  
538 at elevations <500 m. The preferred ME (RME) over elevations 500 m to 1500 m and elevations > 500 m was obtained  
539 using SEBS and FLADS, respectively, see Table 5 (level one: 24–26).

540

541

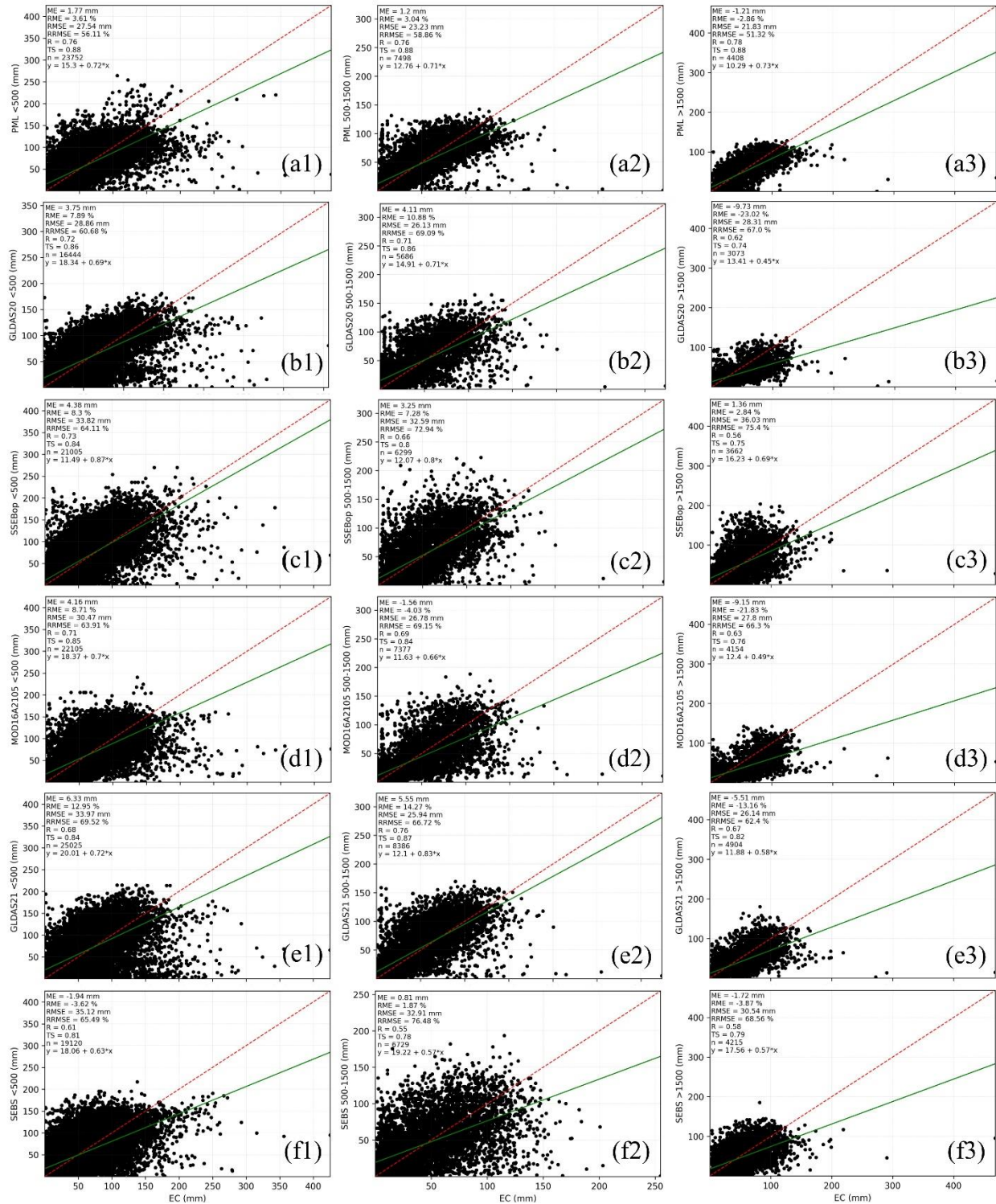
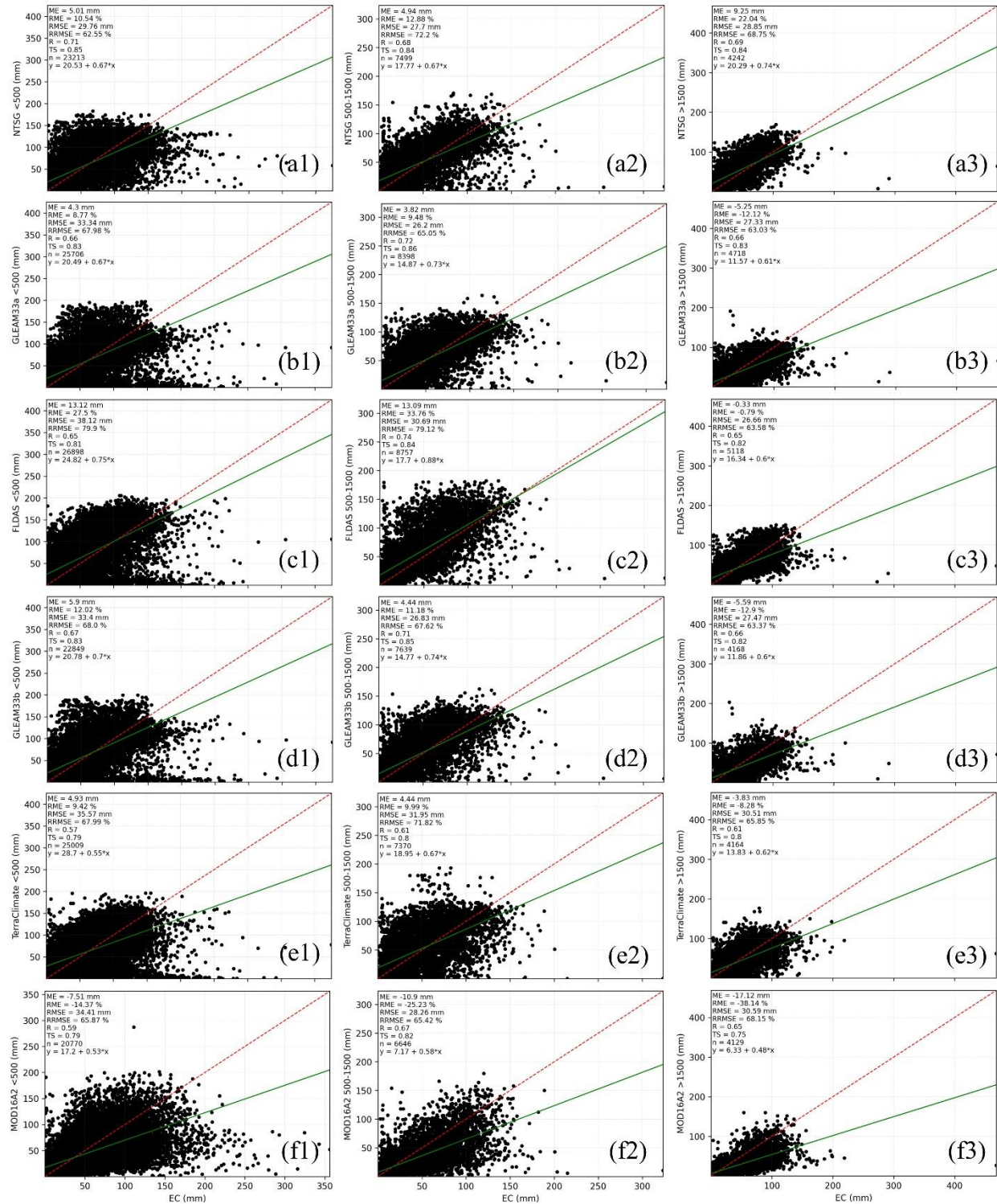


Figure 4011. Monthly ET products (PML: (a); GLDAS20: (b); SSEBop: (c); MOD16A2105: (d); GLDAS21: (e); SEBS: (f)) against flux EC ET aggregated for all sites for each elevation level (<500 m: (1); 500 m–1500 m: (2); >1500 m: (3)).

542  
543  
544  
545  
546





**Figure 1412.** Monthly ET products (NTSG: (a); GLEAM33a: (b); FLDAS: (c); GLEAM33b: (d); TerraClimate: (e); MOD16A2: (f)) against flux EC ET aggregated for all sites for each elevation level (<500 m: (1); 500 m–1500 m: (2); >1500 m: (3)).

547  
548  
549

---

## 550 4.2. Ensemble ET product

### 551 4.2.1. Ensemble steps

552 Table 5 provides levels one and two validation metrics of all ET products for monthly (01), annual (02),  
553 interannual (January-December: 03–14), land cover types (croplands, grasslands, forests, water bodies, others: 15–  
554 19), climatic classes (arid, semiarid, dry sub-humid, humid: 20–23), and elevation levels (<500 m, 500 m-1500 m,  
555 >1500 m: 24–26). Each cell represents one of the validation levels (01–26) and the best-performing ET product based  
556 on the selected validation metric, see Sect. 3.

557 Table 6 shows that, according to ~~first-the occurrence of ET products in~~ level ~~accuracy~~one, PML, GLDAS20,  
558 and SEBS represent the first three best-performing ET products, while according to the ~~second occurrence of ET~~  
559 ~~products in~~ level two GLDAS20, PML, and MOD16A2105, and according to the total ~~of the first and~~  
560 ~~second occurrence in~~ levels one and two, PML, GLDAS20, and SSEBop are the best, respectively. For example, PML  
561 yielded the best validation ~~indices~~metrics (the lowest ME, RME, RMSE, and RRMSE as well as the highest R and  
562 TS) over 83 (53%) and 24 (15%) cells in levels one and two, respectively; thus, the total count was 107 (34%) cells.  
563 Accordingly, the three best-performing ET products over most of the all conditions are MPL followed by GLDAS20  
564 (~~first-level~~ one: 10 (6%); ~~second-level~~ two: 37 (24%); total: 37 (15%)) and SSEBop (~~first-level~~ one: 12 (8%); ~~second~~  
565 level two: 15 (10%); total: 27 (9%)).

566 Since the three best-performing ET products differ in their spatial resolution and algorithms, we introduced  
567 an ensemble mean product at a 1000 m × 1000 m spatial resolution that spans from 2003 to 2017 (15 years) and relies  
568 on remotely sensed models (PML and SSEBop). It should be noted that although SEBS has one point more than  
569 SSEBop ~~in the first on~~ level one, it has 7 fewer points than SSEBop in ~~the second-level~~ two (5%). In addition, SSEBop  
570 has a higher spatial resolution than that of SEBS. In the same manner, SSEBop and MOD16A2105 have the same  
571 performance in terms of total count (27 (9%)), but SSEBop is higher by 5 points in ~~the first-level~~ one.

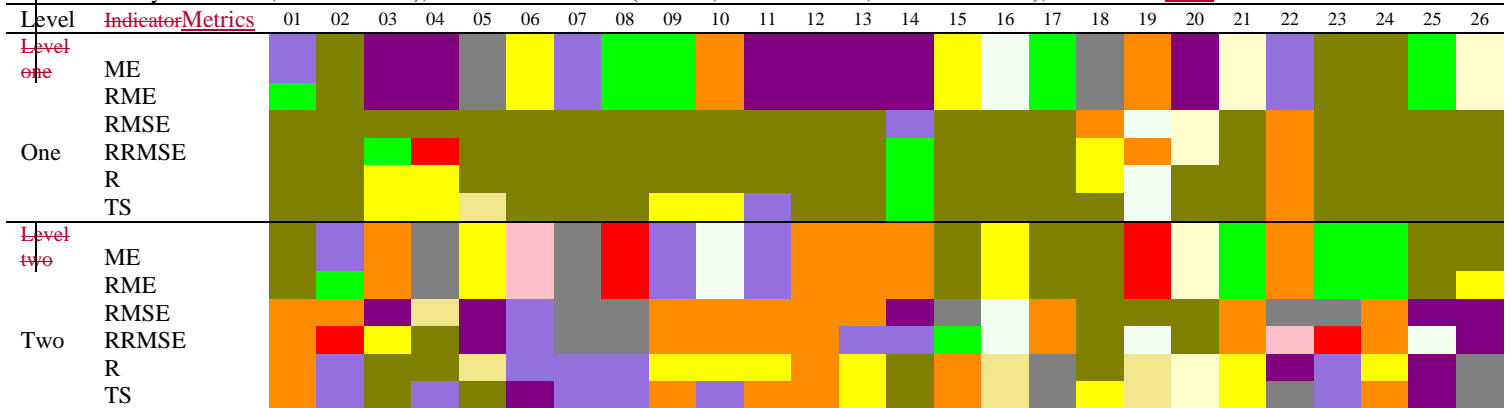
572 Obviously, from Table 7, the ensemble ET products cannot perform highly across all regions, and it had a  
573 total count of 50%, followed by PML (44%). Looking to the ensemble mean from Table 7 compared to PML from  
574 Table 6, the total count increased from 34% to 50% (+16%), indicating that the ensemble mean, which created from  
575 PML and SSEBop, enhanced PML performance across all conditions by 16% and PML itself still has the best  
576 performance by 44%.

577 To introduce an ensemble product before 2003, firstly, PML and SSEBop were ignored, and the same steps  
578 were repeated. Table 8 shows that the best-performing products are GLDAS20, MOD16A2105, and NTSG in terms  
579 of the total count. Since the last two products are based on remote sensing, they were selected to create the ensemble  
580 product before 2003 at a 1000 m × 1000 m spatial resolution. Although GLDAS20 agreed well over 42% and had the  
581 lowest maximum ME among all datasets (9.73 mm), NTSG was selected to provide the ET estimates before 2000  
582 because it had a higher spatial resolution, so it could capture more spatial details than GLDAS20.

583 Table 9 shows that the ensemble ET for 2001 and 2002 performed better than the original ET products, with  
584 values of 62%, 38%, and 50% for level one, level two and the total, respectively. For the periods before 2001, NTSG  
585 can be used from 1982 to 2001 or GLDAS20 can be used instead. Hence, remotely sensed-based long-term ensemble

586 ET can be synthesized from PML and SSEBop between 2003 and 2017, MOD16A2105 and NTSG between 2001 and  
 587 2002. SSEBop can be used after 2018, while before 2000, NTSG can be used.

588 **Table 5.** Levels one and two validation metrics of all the 12 ET products for monthly (01), annually (02) interannual (January-  
 589 December: 03-14), land cover types (croplands, grasslands, forests, water bodies, others: 15-19), climatic classes (arid, semiarid,  
 590 dry sub-humid, humid: 20-23), and elevation levels (<500 m, 500 m-1500 m, >1500 m: 24-26), cells colour color as Table 6.



591  
 592 **Table 6.** The count, percent and occurrence of the total count and percent of levels one and two of all 12 ET products  
 593 performance based on Table 5.

ET products	Occurrence in level 1		Occurrence in level 2		Total	
	Level 1 count	Level 1 count (%)	Level 2 count	Level 2 count (%)	Total count	% Total count (%)
PML	83	53	24	15	107	34
GLDAS20	10	6	37	24	47	15
SSEBop	12	8	15	10	27	9
MOD16A2105	7	4	20	13	27	9
GLDAS21	14	9	11	7	25	8
SEBS	13	8	8	5	21	7
NTSG	4	3	16	10	20	6
GLEAM33a	5	3	6	4	11	4
FLDAS	6	4	4	3	10	3
GLEAM33b	1	1	6	4	7	2
TerraClimate	1	1	6	4	7	2
MOD16A2	0	0	3	2	3	1

594  
 595 **Table 7.** The count, percent and the total count and percent of levels one and two occurrence of PML and SSEBop products and  
 596 their ensemble mean for the period during 2003- and 2017.

ET products	Occurrence in level 1		Occurrence in level 2		Total	
	Level 1 count	Level 1 count (%)	Level 2 count	Level 2 count (%)	Total count	% Total count (%)
Mean	43	28	113	72	156	50
PML	103	66	33	21	136	44
SSEBop	10	6	10	6	20	6

597  
 598  
 599  
 600  
 601  
 602  
 603

604 **Table 8.** The count, percent and the total count and percent of levels one and two occurrence of all ET products performance  
 605 except PML and SSEBop products.

ET products	Occurrence in level 1		Occurrence in level 2		Total	
	Level 1 count	Level 1 count (%)%	Level 2 count	Level 2 count (%)%	Total count	Total count (%)%
GLDAS20	42	27	27	17	69	22
MOD16A2105	28	18	28	18	56	18
NTSG	14	9	35	22	49	16
GLDAS21	23	15	14	9	37	12
SEBS	21	13	7	4	28	9
GLEAM33a	8	5	16	10	24	8
GLEAM33b	6	4	15	10	21	7
FLDAS	9	6	5	3	14	4
TerraClimate	3	2	5	3	8	3
MOD16A2	2	1	4	3	6	2

606 **Table 9.** The count, percent and the total count and percent of levels one and two occurrence of NTSG and MOD16A2105  
 607 products and their ensemble mean for during 2001 and 2002.

ET products	Occurrence in level 1		Occurrence in level 2		Total	
	Level 1 count	Level 1 count (%)%	Level 2 count	Level 2 count (%)%	Total count	Total count (%)%
Mean	96	62	59	38	155	50
NTSG	19	12	68	44	87	28
MOD16A2105	41	26	29	19	70	22

#### 608 4.2.2 Contribution of ET datasets to the synthesized ET

609 The synthesized ET dataset was created at a 1000 m × 1000 m spatial resolution from 1982 to 2019 based on  
 610 remotely sensed ET products. PML, SSEBop, MOD16A2105, and NTSG were augmented together to create the new  
 611 dataset. Since SSEBop and MOD16A2105 have a 1000 m × 1000 m spatial resolution, PML was upscaled and NTSG  
 612 was downscaled by pixel average and nearest neighbor resampling techniques in GEE, respectively. The synthesized  
 613 ET was fully contributed by SSEBop for the years 2018 and 2019 and by NTSG from 1982 to 2000, while for the  
 614 years 2001 and 2002, it was contributed by the simple mean of MOD16A2105 and NTSG. Finally, between 2003 and  
 615 2017, the value represents the simple mean of PML and SSEBop.

616 Since the synthesized ET performance was governed by each ET product(s) for the corresponding year from  
 617 1994 to 2019 (25 years), where the ET EC fluxes were available, most of the performance comes from PML and  
 618 SSEBop for the 15 years from 2003 to 2017 (60%), from MOD16A2105 and NTSG for 2 years (2001 and 2002; 8%),  
 619 from SSEBop for individual values in years 2018 and 2019 (8%), and from NTSG for 7 years (24%) from 1994 to  
 620 2000.

#### 621 4.2.3. Synthesized global ET product

622 Figure 4-13 shows, looking to July, except over barren land, permanent snow and ice, and arid areas (not  
 623 shown), the maximum value of the synthesized ET lies between SSEBop, which yields the largest ET during all  
 624 months, and PML. Hence, the long-term monthly synthesized ET performance is affected by PML and SSEBop more  
 625 than by NTSG and MOD16A2105, as mentioned in Sect. 4.2.2.

626 Table 10 provides the average monthly and annual synthesized ET (mm month<sup>-1</sup>), land cover types, aridity  
 627 index classes, and elevation levels (mm year<sup>-1</sup>). The average annual ET from 1982–2019 is 567 mm year<sup>-1</sup>. July

---

628 represents the maximum synthesized ET (Fig. 4213). Table 10 also provides average annual ET for land cover types  
629 calculated from flux sites. Across land cover types, croplands are higher than forests, followed by grassland, where  
630 the average synthesized ET was 597, 548, and 542 for croplands, forests, and grasslands, respectively. Low  
631 synthesized ET values across arid areas (average = 392 mm year<sup>-1</sup>) can be attributed to low vegetation cover. It should  
632 be noted that Table 10 does not represent the perfect calculation of ET over each Land cover class because the total  
633 number of fluxes for each class was not distributed well; for instance, in the arid areas, there were 35 (5%) fluxes,  
634 while in the humid area, there were 361 (56%) fluxes.

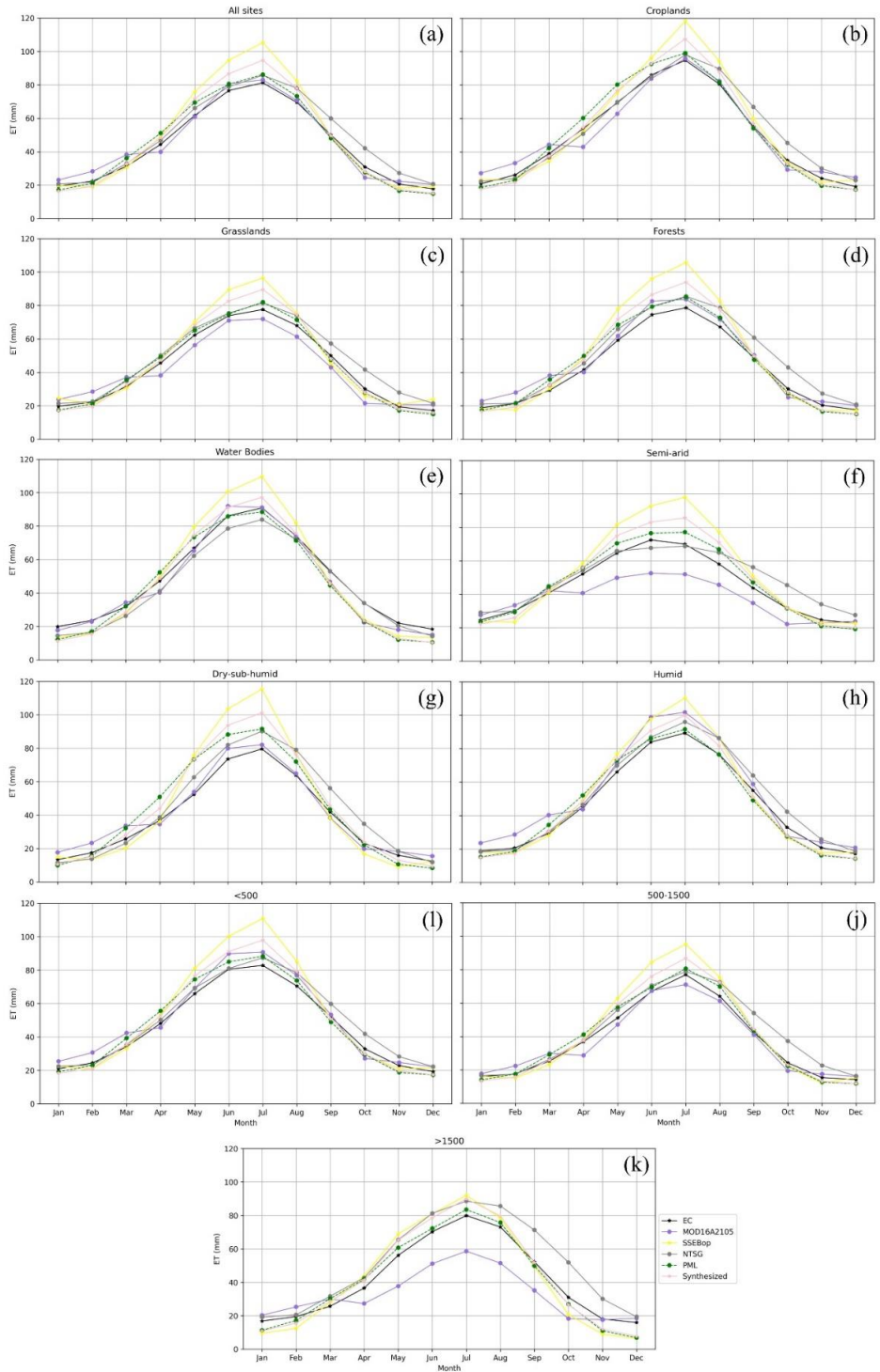
635 Figure 43-14 shows the decadal (1982–1989, 1990–1999, 2000–2009, and 2010–2019) and long-term (1982–  
636 2019) average synthesized ET maps worldwide, except for Antarctica. Regarding the spatial distribution, the higher  
637 ET is shown in Malaysia, Singapore, and Indonesia and the northern part of South America. During the first and  
638 second decades, the synthesized ET is based on the NTS product; thus, the same spatial distribution was observed.  
639 Although PML and SSEBop mainly contribute the synthesized ET between 2003 and 2017, there is little difference  
640 in their spatial distributions, where higher ET can be observed during 2010–2019 over the northern parts of South  
641 America.

642 Table 11 shows statistics of the maps provided in Fig. 43-14 for all continents except Antarctica. The standard  
643 deviation is higher over Africa followed by Oceania and Asia. The mean values of the synthesized ET is sequenced  
644 from South America followed by Oceania and Africa. The maximum value of the synthesized ET is recorded over  
645 Asia followed Africa and Australia. The total ETs are 29.1%, 21.7%, 19.9%, 16.7%, 7.9%, 4.2%, and 0.5% for Asia,  
646 South America, Africa, North America, Europe, Australia, and Oceania, respectively.

#### 647 4.2.4 Validation of the synthesized ET

648 Figures 4415–47-18 show that the synthesized ET agreed well with the observed data, where the R (TS)  
649 ranged between 0.70 (0.85) and 0.78 (0.89), except at the annual time step (Fig. 44b15b) and over barren land and  
650 permanent snow and ice (not shown), where R (TS) was 0.65 (0.81) and 0.68 (0.80), respectively. Based on the ME  
651 sign, the value was underestimated only over water bodies. The magnitude of ME (RME) ranged between 0.54 mm  
652 (1.05%) and 6.76 mm (16.62%), while the RMSE (RRMSE) ranged from 20.95 mm (45.22%) to 30.12 mm (59.61%).  
653 Looking at the regression line equation, with no exceptions, the synthesized ET overestimated the flux EC ET at lower  
654 ET values and underestimated the flux EC ET at higher ET values. As mentioned above, even the long-term  
655 synthesized ET cannot perform best across all comparison levels (Tables 12 and 13).

656 During the periods 2018–2019 and before 2001, the synthesized ET performance came from the original  
657 datasets of SSEBop and NTS product, respectively. The ensemble mean has a total count of 50% over the periods 2003–  
658 2017 and 2001–2002 compared to the original datasets, indicating that it can perform better than other ET products  
659 over half of all comparison levels, see Tables 7 and 9.



660  
661  
662  
663  
664

**Figure 123.** Monthly average synthesized ET and the original products over all flux sites (a), land cover types (croplands: (b); grasslands: (c); forests: (d); water bodies: (e)), climate classes (semiarid: (f); dry sub humid: (g); humid: (h)), and elevation levels (<500 m: (i), 500 m-1500 m: (j), and >1500m: (k)) Monthly average flux EC ET, MOD16A2105, SSEBop, NTSG, PML and the synthesized ET (subplot label as in Figure 3):

665

666

667  
668

**Table 10.** The average decadal synthesized ET of monthly (mm month<sup>-1</sup>) and land cover types, aridity index classes and elevation levels (mm year<sup>-1</sup>).

Level	1982–1989	1990–1999	2000–2009	2010–2019	1982–2019
January	43.22	44.10	44.94	45.99	44.56
February	39.73	41.14	42.83	42.09	41.45
March	44.83	45.09	43.73	42.93	44.15
April	45.84	46.04	39.32	38.57	42.44
May	52.86	53.36	47.13	46.61	49.99
June	56.15	57.31	53.98	54.00	55.36
July	60.83	61.80	57.06	56.99	59.17
August	58.02	58.77	51.25	50.25	54.57
September	49.99	50.15	44.10	42.79	46.76
October	46.76	46.91	38.53	38.77	42.74
November	42.55	42.45	41.52	42.29	42.20
December	42.66	43.58	42.92	44.43	43.40
Annual	583	591	547	546	567
Croplands	597	619	595	577	597
Grasslands	526	546	539	557	542
Forests	541	561	544	546	548
Water bodies	499	517	519	534	517
Others	280	288	230	195	248
Arid	400	405	366	398	392
Semiarid	519	538	528	541	532
Dry sub-humid	479	498	498	511	497
Humid	577	600	582	577	583
Elevation <500m	551	570	570	579	568
Elevation 500 m – 1500 m	498	519	484	484	496
Elevation >1500 m	557	583	506	471	529

669 Note: Monthly and annual estimates have based on synthesized ET raster layers averaged over a decade. Land cover  
670 types, aridity index classes and elevation levels estimates have based on annual synthesized ET values extracted over  
671 all flux sites.

672

673

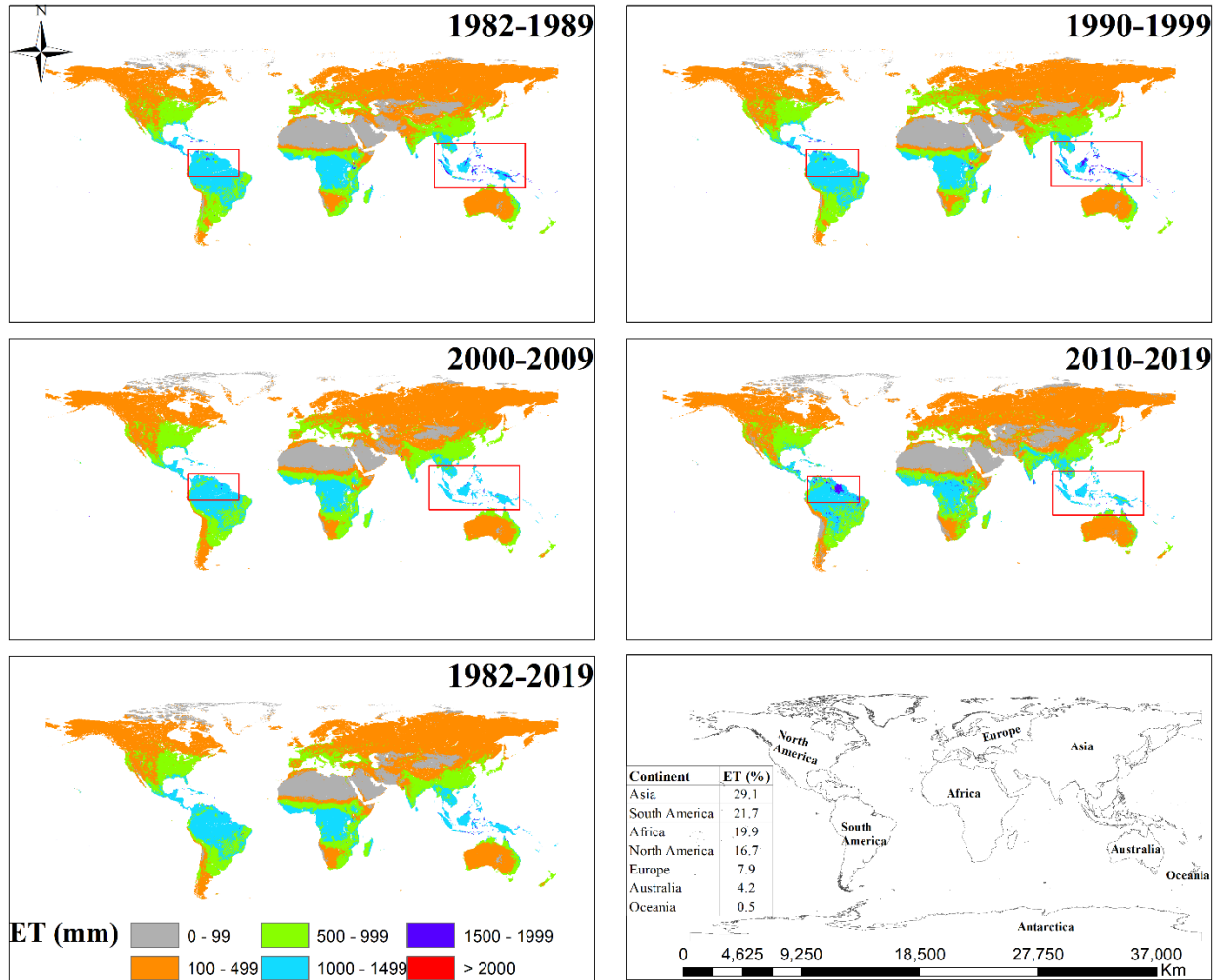
674

675

676

677

678



679  
 680 **Figure 1314.** Decadal and long-term synthesized ET, the last plot shows continental-scale used to create Table 1311 accompanied  
 681 by the percent of ET over each continent for the periods 1982–2019 except Antarctica. Use the following link of the GEE  
 682 application to preview these maps: <https://elnashar.users.earthengine.app/view/synthesizedet/>

683  
 684  
 685  
 686  
 687  
 688  
 689  
 690  
 691  
 692  
 693



694

695 **Table 11.** Statistics of the decadal and long-term synthesized ET (mm).

Period	Continent	Minimum	Maximum	Mean	Standard Deviation	Sum
1982-1989	Africa	0	3588	541	540	17091316777
	Asia	0	3979	377	392	25075224084
	Australia	0	4076	445	275	3812181627
	Europe	0	2934	403	189	6902627799
	North America	0	3818	413	331	14682344407
	Oceania	111	2155	903	392	431987028
	South America	4	3585	1002	364	18968179507
	Global	0	4076	583	355	86963861230
1990-1999	Africa	0	3673	555	545	17552175432
	Asia	0	4054	387	398	25755440497
	Australia	0	4240	438	281	3748291789
	Europe	0	2825	424	203	7260038441
	North America	0	3742	423	338	15051753185
	Oceania	111	2176	892	394	426754913
	South America	8	3409	1015	363	19218216796
	Global	0	4240	591	360	89012671053
2000-2009	Africa	0	4326	538	504	17073575117
	Asia	0	4794	393	377	26457856410
	Australia	0	4804	397	260	3417383567
	Europe	0	4108	399	165	7119724411
	North America	0	3915	333	310	15229417841
	Oceania	0	3349	811	398	425095485
	South America	0	3975	960	411	18312021115
	Global	0	4804	547	346	88035073946
2010-2019	Africa	0	4892	556	530	17631809454
	Asia	0	6167	398	401	26760551956
	Australia	0	4692	425	271	3658944492
	Europe	0	3866	384	165	6834742252
	North America	0	4366	338	320	15454707917
	Oceania	0	3387	766	417	391231772
	South America	0	4452	953	453	18166326886
	Global	0	6167	546	365	88898314729
1982-2019	Africa	0	4892	548	530	17337219195
	Asia	0	6167	389	392	26012268237
	Australia	0	4804	426	272	3659200369
	Europe	0	4108	402	180	7029283226
	North America	0	4366	377	325	15104555837
	Oceania	0	3387	843	400	418767300
	South America	0	4452	983	398	18666186076
	Global	0	6167	567	357	88227480239

696

697

698

699

700

701

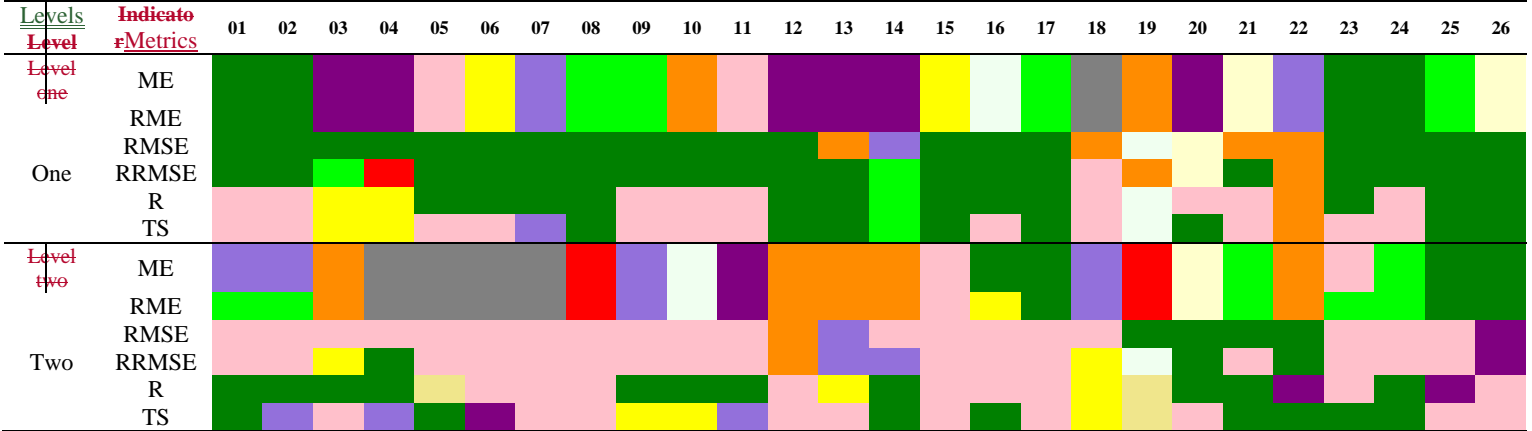
702

703

704

705

706 **Table 12.** Same as Table 5 but Levels one and two validation metrics of all ET products (except MOD16A2) and replaced by the  
 707 synthesized ET for monthly (01), annually (02) interannual (January-December: 03-14), land cover types (croplands, grasslands,  
 708 forests, water Bodies, others: 15-19), climatic classes (arid, semiarid, dry sub-humid, humid: 20-23), and elevation levels (<500  
 709 m, 500 m-1500 m, >1500 m: 24-26). (cells colour as Table 13).



710 Note: MOD16A2 ignored according to Sec. 4.1.

711 **Table 13.** The count, percent and the total count and percent of levels one and two of all ET products (except MOD16A2) and  
 712 Same as Table 6 but MOD16A2 replaced by the synthesized ET performance and based on Table 12.

ET products	Occurrence in level 1		Occurrence in level 2		Total	
	Level 1-count	Level 1-count (%)%	Level 2-count	Level 2-count (%)%	Total-count	Total-count (%)%
PML	66	42	33	21	99	32
Synthesized	26	17	57	37	83	27
GLDAS20	12	8	12	8	24	8
GLDAS21	12	8	7	4	19	6
SEBS	12	8	7	4	19	6
MOD16A2105	6	4	12	8	18	6
SSEBop	8	5	8	5	16	5
NTSG	2	1	8	5	10	3
FLDAS	6	4	2	1	8	3
GLEAM33a	5	3	3	2	8	3
TerraClimate	1	1	4	3	5	2
GLEAM33b	0	0	3	2	3	1

713

714

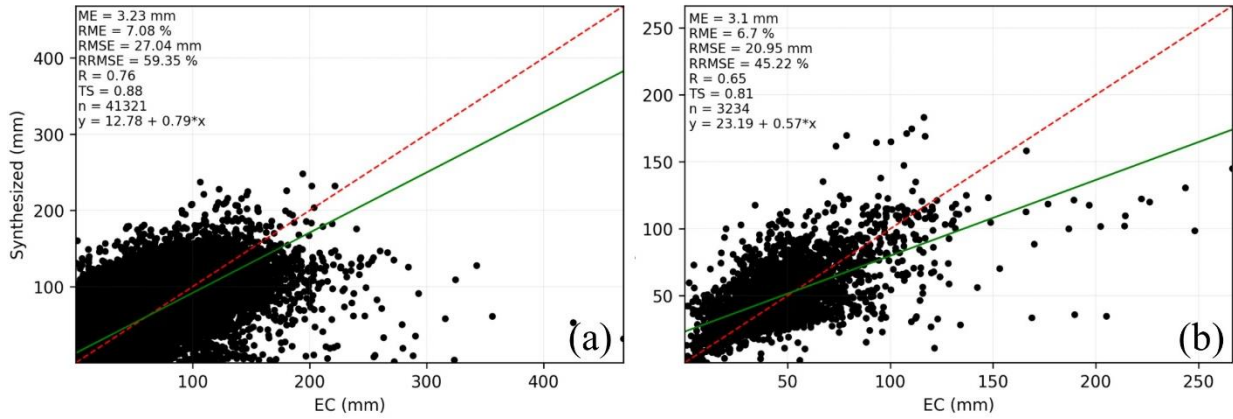
715

716

717

718

719

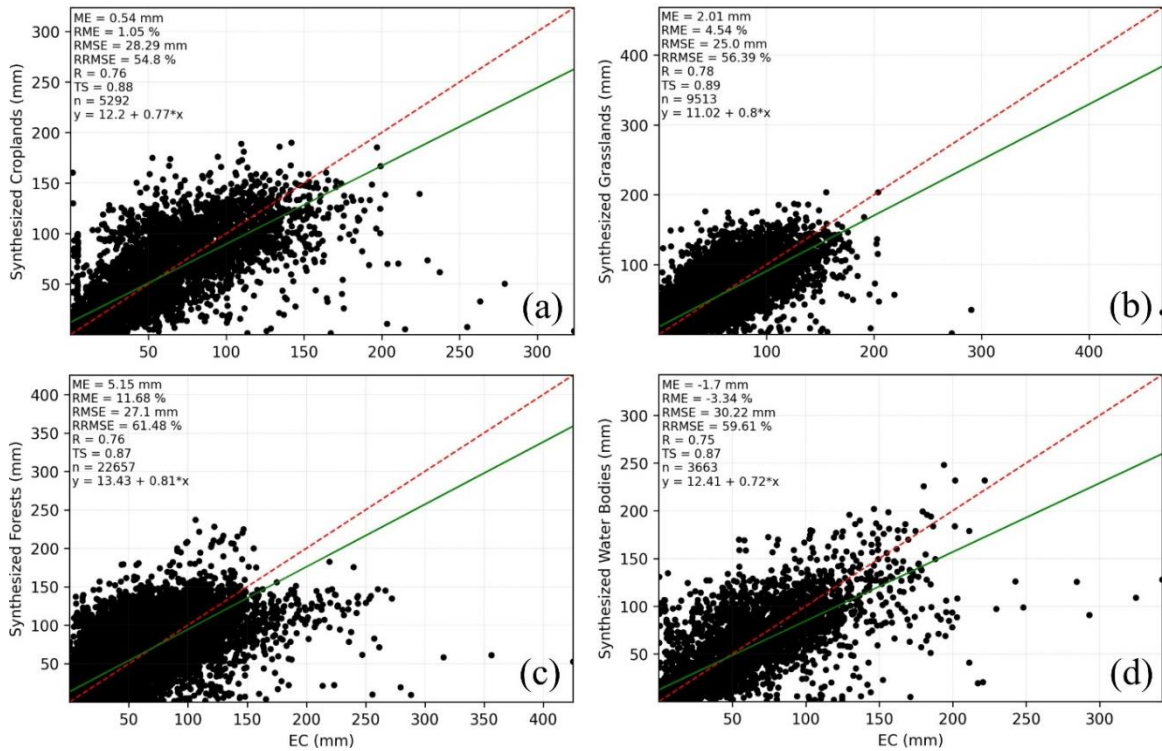


720

721

**Figure 1415.** Monthly (a) and annually (b) synthesized ET against flux EC ET aggregated for all sites.

722



723

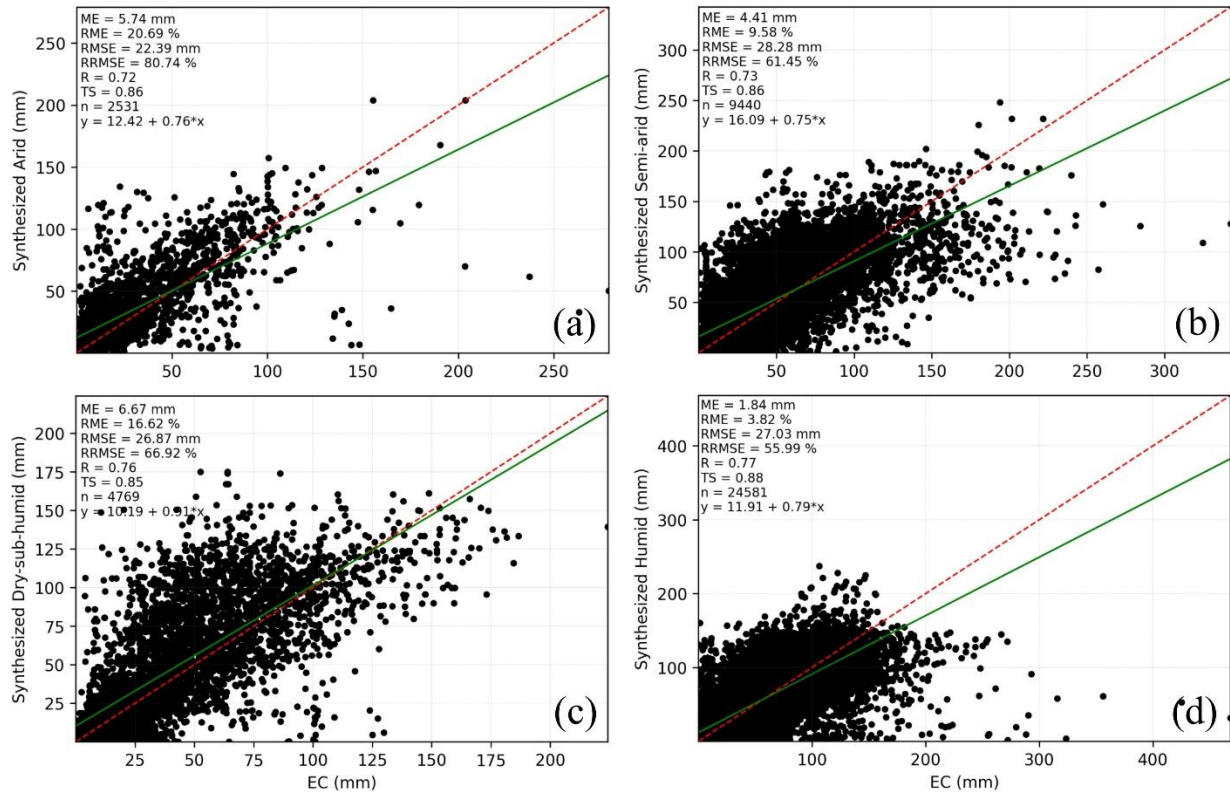
724

725

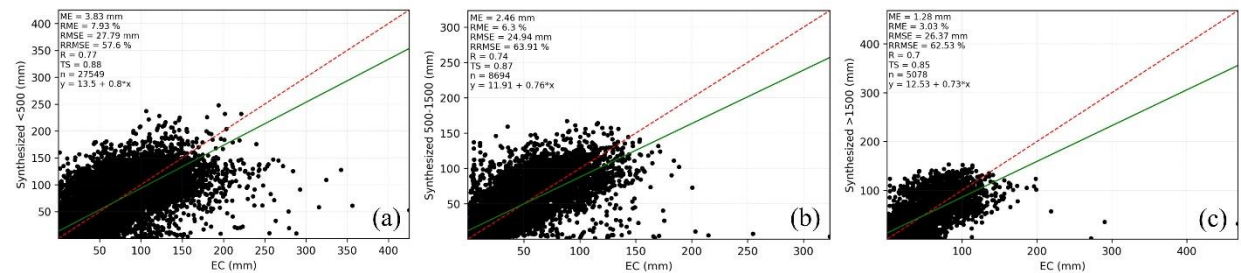
**Figure 1516.** Monthly synthesized ET against flux EC ET aggregated for all sites for each land cover type (croplands: (a); grasslands: (b); forest: (c); water bodies: (d)).

726

727



728  
729 **Figure 1617.** Monthly synthesized ET against flux EC ET aggregated for all sites for each climate class (arid: (a); semiarid: (b);  
730 dry-sub-humid: (c); humid: (d)).



731  
732 **Figure 1718.** Monthly synthesized ET against flux EC ET aggregated for all sites for each elevation level (<500 m: (a); 500 m–  
733 1500 m: (b); >1500 m: (d)).

734 Figure 1819 presents a monthly comparison between the synthesized ET with the country-based ET products  
735 over China and the United States as well as over the African continent. In general, the synthesized ET returned higher  
736 agreement (R and TS) and accuracy (RMSE) with the flux EC ET than did the other ET products (CR, SSEBop, and  
737 FAO WaPOR). Moreover, it has lower biases over the United States and the African continent.

738

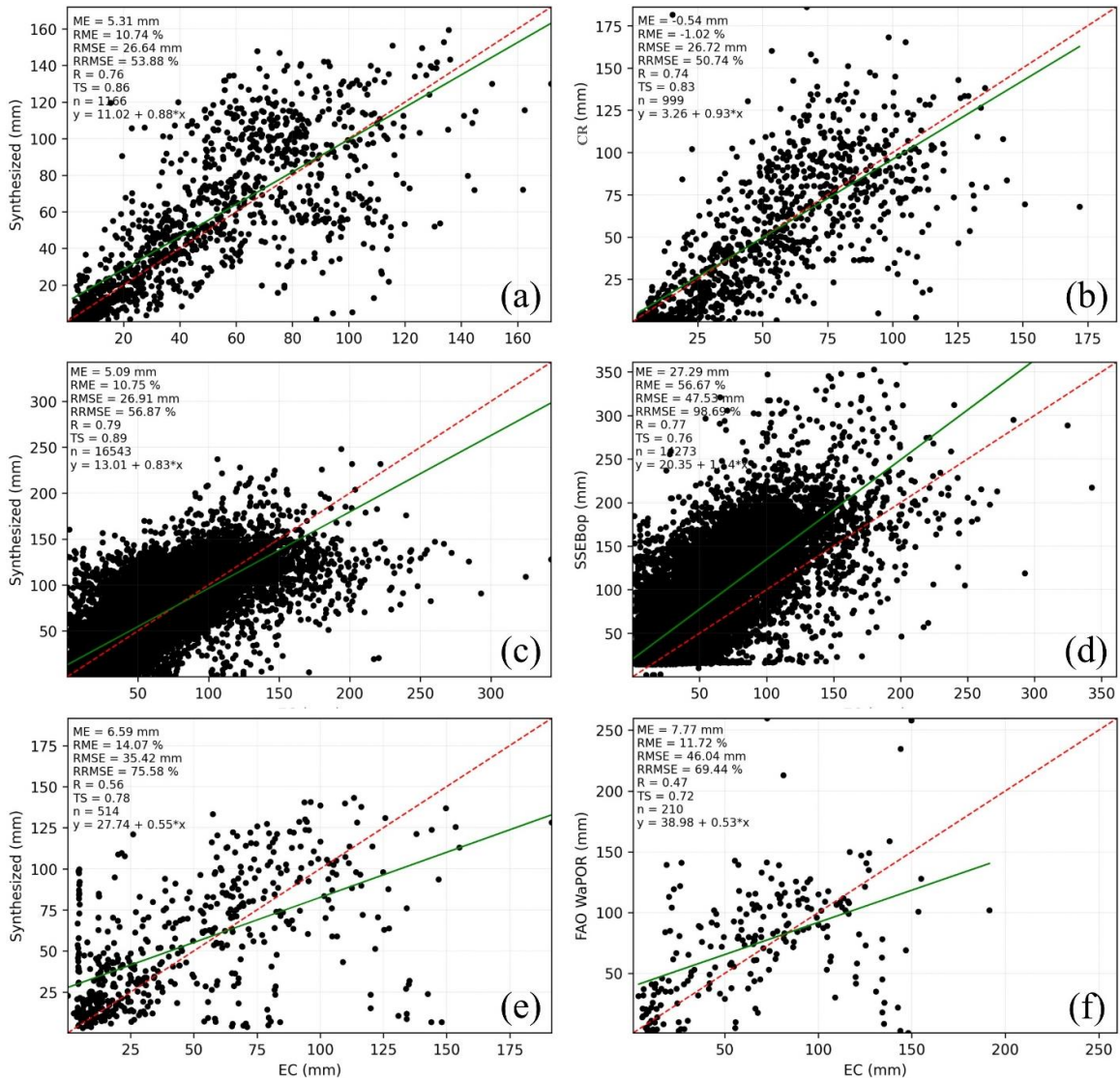


**Figure 1819.** Monthly comparison between the synthesized ET (a, c and e) and CR (b), SSEBop (d), and FAO WaPOR (f) ET products against flux EC ET aggregated for all sites over China (a and b), the USA (c and d) and the African continent (e and f).

## 5. Discussion

Since global land ET plays a paramount role in the hydrological cycle, its accurate estimation is essential for further studies. Although there are many global ET products that have been derived from remote sensing models, land surface models, and hydrological models, they differ in their algorithms, parameterization, and temporal span, and none of these products can be used for a long time with a reasonable spatial resolution and lower uncertainty. In this study, we ensemble the best-performing, currently available global ET products at a reasonable spatial resolution (kilometer) as one consistent global ET dataset covering a long temporal period. Users can use this dataset assuredly without looking at other datasets and performing additional assessments.

We used a high-quality dataset of global flux towers as a site-pixel-level validation for certain global ET products (Leuning et al., 2008; Zhang et al., 2010; Ershadi et al., 2014; Michel et al., 2016) to assess them and select

752 the best products to create a synthesized ET covering a long temporal period. For that, a matrix of 6 validation criteria  
 753 and 26 comparison levels was created, and then levels one and two of the validation metrics were used to select the  
 754 best-performing products. Finally, by the simple mean of the products that performed best over the different periods,  
 755 the synthesized ET was created.

756 Among all global ET products investigated in this study, the products that performed best are PML,  
 757 GLDAS20, SSEBop, MOD16A2105, GLDAS21, SEBS, and NTSG (Table 6). From the perspective of all comparison  
 758 levels, the performance of these products varied, and no single product performed well across all land surface types  
 759 and conditions (Vinukollu et al., 2011a; Li et al., 2018). The PML represents the ET product with the highest  
 760 agreement, with lower ME (RME) and RMSE (RRMSE) values, followed by the synthesized ET (Tables 12 and 13);  
 761 however, it should be noted that PML estimates span a 15-yr period, while the synthesized ET presents longer  
 762 estimates from 1982 to 2019 (38 years).

763 The main advantage of the new dataset is that, for the first time, a synthesized remotely sensed ET product  
 764 with a reasonable spatial resolution and lower long-term uncertainties has been provided, where the maximum absolute  
 765 ME (RME) and RMSE (RRMSE) values are 13.94 mm (17.13%) and 38.61 mm (47.45%), respectively. Furthermore,  
 766 it agreed well ( $R > 0.70$ ) in 62% of all comparison levels (Table 14). This dataset can provide ensemble ET estimates  
 767 for all land cover types, where MOD16A2105 does not provide ET estimates over water bodies and desert areas other  
 768 products are. Moreover, a comparison among the synthesized ET against CR, SSEBop, and FAO WaPOR ET products  
 769 over China, the United States, and the African continent proved that the synthesized ET outperformed these products  
 770 in terms of a higher agreement, higher accuracies and lower biases. Hence, the synthesized ET can play an essential  
 771 role, especially for regional and global scale studies, over a long time (1892–2019).

772 **Table 14.** Percentage of R more than 0.70 and the maximum absolute value of ME (mm), RME (%) RMSE (mm), and RRMSE  
 773 (%) across all comparisons levels (01–26) of the highly preformed ET products and the synthesized ET.

ET products	R>0.7 (%)	ME	RME	RMSE	RRMSE
PML	65	7.64	12.22	36.28	44.30
Synthesized	62	13.94	17.13	38.61	47.45
GLDAS20	42	9.73	23.02	39.53	49.32
SSEBop	42	21.82	26.07	48.14	57.50
MOD16A2105	42	12.89	51.06	42.78	53.27
GLDAS21	35	13.69	22.07	47.84	58.32
NTSG	23	14.46	86.35	40.50	50.26

774 The synthesized ET used SSEBop ET for the years 2018 and 2019 and NTSG from 1982 to 2000 because  
 775 NTSG is the only remotely sensed global ET product available and has a good spatial resolution compared to  
 776 GLDAS20. It is the simple mean of MOD16A2105 and NTSG for the years 2001 and 2002 and the simple mean of  
 777 PML and SSEBop between 2003 and 2017 (see Tables 7 and 9).

778 Because the ET was synthesized during the first and second decades as well as the year 2000 based on  
 779 resampled NTSG to a 1 km spatial resolution to be comparable with other products, future improvements may be  
 780 focused on statistical downscaling of NTSG during this period. Moreover, since different datasets were selected due  
 781 to enhanced data availability, also future improvements may be focused on the product proposed in this paper adjustment  
 782 of the ensemble means particularly for long-term pixel-based studies.

---

## 783 6. Data availability

784 All data used in this study are freely available; see Sect. 2 and Appendix A. The synthesized ET is available  
785 in <https://doi.org/10.7910/DVN/ZGOUED> (Elnashar et al., 2020) and as GEE application from the following link:  
786 <https://elnashar.users.earthengine.app/view/synthesizedet>. In addition, it can be accessed in the GEE JavaScript editor  
787 (the updated link embedded in the GEE application interface). Through this application, the user can query and display  
788 as well as download the synthesized ET. It should be noted that SSEBop and NTSG datasets are not available in Earth  
789 Engine so they were uploaded as assets in GEE for this purpose.

## 790 7. Conclusion

791 In the current study, a site-pixel-level validation was conducted for certain global ET products across a variety  
792 of land surface types and conditions to select the best performing ET products and then produce a global long-term  
793 synthesized ET dataset. To apply a comprehensive evaluation from different perspectives, land cover types, climate  
794 and elevations were classified into five, four, and three classes, respectively. According to six comprehensive  
795 validation criteria, the evaluated ET products ranked based on the lowest error metrics and highest accuracy and  
796 consistency over different classification levels to choose the ensemble members over different times.

797 ~~Concerning the study investigation, PML, GLDAS20, SSEBop, MOD16A2105, GLDAS21, SEBS,~~  
798 ~~and NTSG were ET products that performed best. The average annual ET from 1982–2019 is 567 mm year<sup>-1</sup>. Although~~  
799 ~~no product performed best~~ in terms of all selected validation criteria in all classification levels, ~~the PML,~~  
800 ~~GLDAS20, SSEBop, MOD16A2105, GLDAS21, SEBS, and NTSG are the sequence of their performances. The~~  
801 ~~synthesized ET produced from PML, SSEBop, MOD16A2105 and NTSG had high~~ agreed with the flux EC ET with  
802 ~~R-values higher than 0.70, a maximum ME (RME) of 13.94 mm (17.13%) and a maximum RMSE (RRMSE) of 38.61~~  
803 ~~mm (47.45%) over 62% of all comparisons levels, as remotely sensed based ET product spanning from 1982 to 2019~~  
804 ~~with highest~~ agreements and accuracies with low and lower biases over most of the land surface types and conditions.  
805 ~~In addition, this study provides ET estimates from 1982 to 2019 and for all land cover types. Furthermore, it~~  
806 ~~performed~~ It performs well when compared with country-based and continental ET products over China, the United  
807 States and the African continent. ~~However, the further synthesis of local ET products is encouraged if regional ET~~  
808 ~~products are available.~~

809 The results from this study provide a better understanding of the high performing ET products in each land  
810 cover type, elevation level and climate region as well as a monthly, annual and interannual time steps. Hence, this  
811 study provides an ET product that can be used to improve the quality of ET at regional and global levels and,  
812 consequently, can be used to improve agriculture, water resource management, and climate change studies.

813 **Author Contribution:** Abdelrazek Elnashar was responsible for experimental designing, manuscript preparation, and  
814 data processing and presentation. Linjiang Wang, Dr. Weiwei Zhu, and Dr. Hongwei Zeng contributed to data  
815 processing. Prof. Dr. Bingfang Wu contributed to conceptual designing, reviewing of the manuscript, funding  
816 acquisition, and project administration.

---

817 **Acknowledgments:** This research was financially supported by the National Key Research and Development Program  
818 of China (Grant No. 2016YFA0600303), the National Natural Scientific Foundations of China (grant numbers:  
819 41991232) and the Key Research Program of Frontier Sciences, CAS (grant numbers: QYZDY-SSW-DQC014).  
820 **Conflicts of Interest:** The authors declare that they have no conflict of interest.

## 821 **Appendix A**

822 A summary of ET datasets used in this research is presented here. It should be noted that except for SSEBop,  
823 SEBS, NTSG ET, and GLEAM, which are downloaded from their providers, other datasets are available in Earth  
824 Engine Data Catalog through the following link <https://developers.google.com/earth-engine/datasets/catalog/>. Each  
825 dataset in GEE has Earth Engine Snippet as following:

```
826 MOD16A2 ET V6: ee.ImageCollection("MODIS/006/MOD16A2")  
827 MOD16A2 ET V105: ee.ImageCollection("MODIS/NTSG/MOD16A2/105")  
828 PML ET: ee.ImageCollection("CAS/IGSNRR/PML/V2")  
829 GLDAS ET V20: ee.ImageCollection("NASA/GLDAS/V20/NOAH/G025/T3H")  
830 GLDAS ET V021: ee.ImageCollection("NASA/GLDAS/V021/NOAH/G025/T3H")  
831 FLADS ET: ee.ImageCollection("NASA/FLDAS/NOAH01/C/GL/M/V001")  
832 TerraClimate ET: ee.ImageCollection("IDAHO_EPSCOR/TERRACLIMATE")
```

## 833 **MOD16 ET**

834 The Moderate Resolution Imaging Spectroradiometer (MODIS) Global Evapotranspiration Project  
835 (MOD16A2) estimates terrestrial ET as the sum of evaporation and plant transpiration. MOD16A2 ET uses the  
836 Penman-Monteith model, which includes MODIS remotely sensed data (e.g., vegetation, surface albedo, and land  
837 cover classification) and daily meteorological reanalysis. There are two products of MOD16A2 ET (V6 and V105)  
838 with an 8-day temporal resolution, but they differ in their spatial resolution and temporal coverage (Mu et al., 2011; Mu  
839 et al., 2014b). V6 spans from 2001 until now with a 500 m × 500 m spatial resolution and is provided by NASA LP  
840 DAAC at the USGS EROS Center; it can be downloaded from <https://doi.org/10.5067/MODIS/MOD16A2.006/>.  
841 V105 estimates span the period from 2001 to 2014 with a 1000 m × 1000 m spatial resolution and are provided by the  
842 Numerical Terradynamic Simulation Group (NTSG) at the University of Montana in conjunction with the NASA  
843 Earth Observing System (Mu et al., 2014a).

## 844 **PML ET**

845 The Penman-Monteith Leuning (PML) ET product partitions ET into three components: plant transpiration,  
846 soil evaporation, and intercepted rainfall by the canopy as well as water evaporation. PML data span from 2002 to  
847 2017 with a 500 m × 500 m spatial resolution and an 8-day temporal resolution (Zhang et al., 2019).



---

848 **SSEBop**

849 The operational Simplified Surface Energy Balance (SSEBop) model is based on the Simplified Surface  
850 Energy Balance (SSEB) approach with a unique parameterization for operational applications. Using a thermal index  
851 approach, it combines ET fractions generated from remotely sensed MODIS land surface temperature, acquired every  
852 10 days, with reference ET from global weather datasets. The SSEBop uses predefined, seasonally dynamic, boundary  
853 conditions that are unique to each pixel for the hot and cold reference points (Senay et al., 2007; Senay et al.,  
854 2011; Senay et al., 2013; Senay et al., 2020). SSEBop estimates are from 2003 with a  $0.0096^{\circ} \times 0.0096^{\circ}$  ( $\approx 1$  km) spatial  
855 resolution and a monthly temporal resolution. Data were provided by The Early Warning and Environmental  
856 Monitoring Program via the United States Geological Survey and can be downloaded from the following website  
857 <https://earlywarning.usgs.gov/>.

858 **SEBS**

859 The Surface Energy Balance System (SEBS) is an approach designed to estimate ET from the evaporative  
860 fraction using satellite remote sensing augmented with meteorological data at corresponding scales (Su, 2002).  
861 MODIS-LST and the Normalized Difference Vegetation Index (NDVI), GLASS-LAI, GLAS global forest height,  
862 GlobAlbedo, and ERA-Interim meteorological data have been used in these ET calculations with the revised SEBS  
863 algorithm (Chen et al., 2013; Chen et al., 2014a; Chen et al., 2019). SEBS is available during the period from 2000 to  
864 2017 with a  $5 \text{ km} \times 5 \text{ km}$  spatial resolution and monthly temporal resolution. It is copyrighted by the Institute of  
865 Tibetan Plateau Research, Chinese Academy of Sciences and is available at <http://en.tpdatabase.cn/>.

866 **NTSG ET**

867 The Numerical Terradynamic Simulation Group (NTSG) ET data are based on an algorithm that estimates  
868 transpiration from the canopy and evaporation from soil using a modified Penman-Monteith model and evaporation  
869 from open water using a Priestley-Taylor model. These algorithms were applied globally using the Advanced Very  
870 High-Resolution Radiometer (AVHRR) Global Inventory Modeling and Mapping Studies (GIMMS) NDVI,  
871 NCEP/NCAR Reanalysis daily surface meteorology, and NASA/GEWEX Surface Radiation Budget Release-3.0 solar  
872 radiation inputs (Zhang et al., 2009; Zhang et al., 2010). NTSG estimates cover a period from 1982 to 2013 at a spatial  
873 resolution of  $8 \text{ km} \times 8 \text{ km}$  and a monthly temporal resolution. It is produced by NTSG at the University of Montana  
874 and can be retrieved from <http://files.ntsug.umt.edu/>.

875 **GLEAM**

876 The Global Land Evaporation Amsterdam Model (GLEAM) is physically based on an algorithm that estimate  
877 ET components separately (i.e., transpiration, interception loss, bare soil evaporation, snow sublimation, and open-  
878 water evaporation). The potential evaporation is estimated by the Priestley and Taylor equation based on observations  
879 of surface net radiation and near-surface air temperature and is then converted into actual evaporation based on the  
880 evaporative (soil) stress factor. The soil stress factor is based on microwave vegetation optical depth and simulated  
881 root-zone soil moisture calculated from a multilayer water balance model. Separately, interception loss is calculated

---

882 based on vegetation and rainfall observations. There are two datasets available for GLEAM (i.e., v3.3a, and v3.3b)  
883 that differ only in their forcing and temporal coverage. v3.3a spans from 1980 to 2018 and relies on reanalysis radiation  
884 and air temperature, a combination of gauge-based, reanalysis and satellite-based precipitation, and satellite-based  
885 vegetation optical depth, while v3.3b spans from 2003 to 2018, and its forcing factors are the same as v3.3a except  
886 for radiation and air temperature, which are based on remotely sensed data. Both v3.3a and v3.3b estimates are  
887 provided at a monthly temporal resolution and a  $0.25^{\circ} \times 0.25^{\circ}$  ( $\approx 25$  km) spatial resolution (Miralles et al.,  
888 2011b; Miralles et al., 2011a; Martens et al., 2017).

#### 889 **GLDAS ET**

890 The Global Land Data Assimilation System (GLDAS) generates optimal fields of land surface states and  
891 fluxes using advanced land surface modeling and data assimilation techniques by ingesting satellite and ground-based  
892 observational data products. GLDAS Version 2 has two components (GLDAS-2.0 and GLDAS-2.1) with a  
893  $0.25^{\circ} \times 0.25^{\circ}$  ( $\approx 25$  km) spatial resolution and a 3-hour temporal resolution. GLDAS-2.0 is reprocessed with the updated  
894 Princeton Global Meteorological Forcing Dataset and upgraded Land Information System Version 7. The model  
895 simulation was initialized from January 1, 1948, to December 31, 2010, using soil moisture and other state fields from  
896 the LSM climatology for that day of the year. The simulation used the common GLDAS datasets for land cover  
897 (MCD12Q1), land-water mask (MOD44W), and soil texture and elevation (GTOPO30). The GLDAS-2.1 simulation  
898 started on January 1, 2000, and lasted until December 31, 2019, using the conditions from the GLDAS-2.0 simulation.  
899 This simulation was forced with the National Oceanic and Atmospheric Administration (NOAA)/Global Data  
900 Assimilation System (GDAS) atmospheric analysis, disaggregated Global Precipitation Climatology Project (GPCP)  
901 precipitation, and Air Force Weather Agency's AGRicultural METEorological modeling system (AGRMET) radiation.  
902 The MODIS-based land surface parameters were used in the current GLDAS-2.x products, while the AVHRR base  
903 parameters were used in previous GLDAS-2 products before October 2012 (Rodell et al., 2004).

#### 904 **FLDAS ET**

905 The Famine Early Warning Systems Network (FEWS NET) Land Data Assimilation System (FLDAS)  
906 dataset uses remotely sensed and reanalysis inputs to drive land surface models. It includes information on many  
907 climate-related variables, including evapotranspiration, moisture content, humidity, average soil temperature, and total  
908 precipitation rate. For forcing data, this FLDAS dataset uses a combination of the new version of Modern-Era  
909 Retrospective analysis for Research and Applications version 2 (MERRA-2) data and Climate Hazards Group  
910 InfraRed Precipitation with Station data (CHIRPS), a quasi-global rainfall dataset designed for seasonal drought  
911 monitoring and trend analysis (McNally et al., 2017). FLDAS is provided at a  $0.1^{\circ} \times 0.1^{\circ}$  ( $\approx 10$  km) spatial resolution  
912 and monthly temporal resolution during the period 1982–2019.

#### 913 **TerraClimate ET**

914 TerraClimate ET is estimated based on a monthly one-dimensional soil water balance for global terrestrial  
915 surfaces, which incorporates evapotranspiration, precipitation, temperature, and interpolated plant extractable soil

---

916 water capacity. The water balance model is very simple and does not account for heterogeneity in vegetation types or  
917 their physiological responses to changing environmental conditions (Abatzoglou et al., 2018). TerraClimate estimates  
918 are provided at a monthly temporal resolution from 1958 to 2018 and  $0.041^{\circ} \times 0.041^{\circ}$  ( $\approx 5$  km) grid cells.

## 919 References

- 920 Abatzoglou, J. T., Dobrowski, S. Z., Parks, S. A., and Hegewisch, K. C.: TerraClimate, a high-resolution global dataset  
921 of monthly climate and climatic water balance from 1958–2015, *Scientific data*, 5, 170191,  
922 <https://doi.org/10.1038/sdata.2017.191>, 2018.
- 923 Almusaed, A.: Evapotranspiration and Environmental Benefits, in: *Biophilic and Bioclimatic Architecture: Analytical*  
924 *Therapy for the Next Generation of Passive Sustainable Architecture*, edited by: Almusaed, A., Springer London,  
925 London, 167-171, 2011.
- 926 Andam-Akorful, S. A., Ferreira, V. G., Awange, J. L., Forootan, E., and He, X. F.: Multi-model and multi-sensor  
927 estimations of evapotranspiration over the Volta Basin, West Africa, *International Journal of Climatology*, 35, 3132-  
928 3145, <https://doi.org/10.1002/joc.4198>, 2015.
- 929 Arnell, N. W.: Climate change and global water resources, *Global Environmental Change*, 9, S31-S49,  
930 [https://doi.org/10.1016/S0959-3780\(99\)00017-5](https://doi.org/10.1016/S0959-3780(99)00017-5), 1999.
- 931 Arnell, N. W., and Lloyd-Hughes, B.: The global-scale impacts of climate change on water resources and flooding  
932 under new climate and socio-economic scenarios, *Climatic Change*, 122, 127-140, [https://doi.org/10.1007/s10584-](https://doi.org/10.1007/s10584-013-0948-4)  
933 [013-0948-4](https://doi.org/10.1007/s10584-013-0948-4), 2014.
- 934 Ashouri, H., Hsu, K.-L., Sorooshian, S., Braithwaite, D. K., Knapp, K. R., Cecil, L. D., Nelson, B. R., and Prat, O. P.:  
935 PERSIANN-CDR: Daily Precipitation Climate Data Record from Multisatellite Observations for Hydrological and  
936 Climate Studies, *Bulletin of the American Meteorological Society*, 96, 69-83, [https://doi.org/10.1175/bams-d-13-](https://doi.org/10.1175/bams-d-13-00068.1)  
937 [00068.1](https://doi.org/10.1175/bams-d-13-00068.1), 2015.
- 938 Badgley, G., Fisher, J. B., Jiménez, C., Tu, K. P., and Vinukollu, R.: On Uncertainty in Global Terrestrial  
939 Evapotranspiration Estimates from Choice of Input Forcing Datasets, *Journal of Hydrometeorology*, 16, 1449-1455,  
940 <https://doi.org/10.1175/jhm-d-14-0040.1>, 2015.
- 941 Baldocchi, D.: Measuring fluxes of trace gases and energy between ecosystems and the atmosphere – the state and  
942 future of the eddy covariance method, *Global Change Biology*, 20, 3600-3609, <https://doi.org/10.1111/gcb.12649>,  
943 2014.
- 944 Bastiaanssen, W. G. M., Karimi, P., Rebelo, L.-M., Duan, Z., Senay, G., Muthuwatte, L., and Smakhtin, V.: Earth  
945 observation based assessment of the water production and water consumption of Nile basin agro-ecosystems, *Remote*  
946 *Sensing*, 6, 10306-10334, <https://doi.org/10.3390/rs61110306>, 2014.
- 947 Bhattarai, N., Mallick, K., Stuart, J., Vishwakarma, B. D., Niraula, R., Sen, S., and Jain, M.: An automated multi-  
948 model evapotranspiration mapping framework using remotely sensed and reanalysis data, *Remote Sensing of*  
949 *Environment*, 229, 69-92, <https://doi.org/10.1016/j.rse.2019.04.026>, 2019.
- 950 Chen, X., Su, Z., Ma, Y., Yang, K., Wen, J., and Zhang, Y.: An Improvement of Roughness Height Parameterization  
951 of the Surface Energy Balance System (SEBS) over the Tibetan Plateau, *Journal of Applied Meteorology and*  
952 *Climatology*, 52, 607-622, <https://doi.org/10.1175/jamc-d-12-056.1>, 2013.
- 953 Chen, X., Su, Z., Ma, Y., Liu, S., Yu, Q., and Xu, Z.: Development of a 10-year (2001–2010)  $0.1^{\circ}$  data set of land-  
954 surface energy balance for mainland China, *Atmospheric Chemistry and Physics*, 14, 13097-13117,  
955 <https://doi.org/10.5194/acp-14-13097-2014>, 2014a.
- 956 Chen, X., Massman, W. J., and Su, Z.: A Column Canopy-Air Turbulent Diffusion Method for Different Canopy  
957 Structures, *Journal of Geophysical Research: Atmospheres*, 124, 488-506, <https://doi.org/10.1029/2018jd028883>,  
958 2019.
- 959 Chen, Y., Xia, J., Liang, S., Feng, J., Fisher, J. B., Li, X., Li, X., Liu, S., Ma, Z., Miyata, A., Mu, Q., Sun, L., Tang,  
960 J., Wang, K., Wen, J., Xue, Y., Yu, G., Zha, T., Zhang, L., Zhang, Q., Zhao, T., Zhao, L., and Yuan, W.: Comparison  
961 of satellite-based evapotranspiration models over terrestrial ecosystems in China, *Remote Sensing of Environment*,  
962 140, 279-293, <https://doi.org/10.1016/j.rse.2013.08.045>, 2014b.
- 963 Danielson, J. J., and Gesch, D. B.: Global multi-resolution terrain elevation data 2010, 2011-1073, 2011.
- 964 Degefu, D. M., Weijun, H., Zaiyi, L., Liang, Y., Zhengwei, H., and Min, A.: Mapping Monthly Water Scarcity in  
965 Global Transboundary Basins at Country-Basin Mesh Based Spatial Resolution, *Scientific Reports*, 8, 2144-2144,  
966 <https://doi.org/10.1038/s41598-018-20032-w>, 2018.
- 967 Elnashar, A., Wang, L., Wu, B., Zhu, W., and Zeng, H.: Synthesis of Global Actual Evapotranspiration from 1982 to  
968 2019, V1, Harvard Dataverse, <https://doi.org/10.7910/DVN/ZGOUED>, 2020.

969 Ershadi, A., McCabe, M. F., Evans, J. P., Chaney, N. W., and Wood, E. F.: Multi-site evaluation of terrestrial  
970 evaporation models using FLUXNET data, *Agricultural and Forest Meteorology*, 187, 46-61,  
971 <https://doi.org/10.1016/j.agrformet.2013.11.008>, 2014.

972 FAO: WaPOR Database Methodology: Level 1 Data using remote sensing in support of solutions to reduce  
973 agricultural water productivity gaps, Technical Report, FAO, Rome, 2018.

974 FAO: WaPOR V2 Database Methodology. Remote Sensing for Water Productivity Technical Report: Methodology  
975 Series. Rome, FAO., 2020.

976 Farr, T. G., Rosen, P. A., Caro, E., Crippen, R., Duren, R., Hensley, S., Kobrick, M., Paller, M., Rodriguez, E., Roth,  
977 L., Seal, D., Shaffer, S., Shimada, J., Umland, J., Werner, M., Oskin, M., Burbank, D., and Alsdorf, D.: The Shuttle  
978 Radar Topography Mission, *Reviews of Geophysics*, 45, <https://doi.org/10.1029/2005rg000183>, 2007.

979 Ferguson, P. R., and Veizer, J.: Coupling of water and carbon fluxes via the terrestrial biosphere and its significance  
980 to the Earth's climate system, *Journal of Geophysical Research: Atmospheres*, 112,  
981 <http://dx.doi.org/10.1029/2007jd008431>, 2007.

982 Fisher, J. B., Melton, F., Middleton, E., Hain, C., Anderson, M., Allen, R., McCabe, M. F., Hook, S., Baldocchi, D.,  
983 Townsend, P. A., Kilic, A., Tu, K., Miralles, D. D., Perret, J., Lagouarde, J.-P., Waliser, D., Purdy, A. J., French, A.,  
984 Schimel, D., Famiglietti, J. S., Stephens, G., and Wood, E. F.: The future of evapotranspiration: Global requirements  
985 for ecosystem functioning, carbon and climate feedbacks, agricultural management, and water resources, *Water  
986 Resources Research*, 53, 2618-2626, <https://doi.org/10.1002/2016wr020175>, 2017.

987 Foken, T.: The energy balance closure problem: An overview, *Ecological Applications*, 18, 1351-1367,  
988 <https://doi.org/10.1890/06-0922.1>, 2008.

989 Foken, T., Aubinet, M., and Leuning, R.: The Eddy Covariance Method, in: *Eddy Covariance: A Practical Guide to  
990 Measurement and Data Analysis*, edited by: Aubinet, M., Vesala, T., and Papale, D., Springer Netherlands, Dordrecht,  
991 1-19, 2012.

992 Forootan, E., Khaki, M., Schumacher, M., Wulfmeyer, V., Mehrnegar, N., van Dijk, A. I. J. M., Brocca, L., Farzaneh,  
993 S., Akinluyi, F., Ramillien, G., Shum, C. K., Awange, J., and Mostafaie, A.: Understanding the global hydrological  
994 droughts of 2003–2016 and their relationships with teleconnections, *Science of The Total Environment*, 650, 2587-  
995 2604, <https://doi.org/10.1016/j.scitotenv.2018.09.231>, 2019.

996 Funk, C., Peterson, P., Landsfeld, M., Pedreros, D., Verdin, J., Shukla, S., Husak, G., Rowland, J., Harrison, L., and  
997 Hoell, A.: The climate hazards infrared precipitation with stations-a new environmental record for monitoring  
998 extremes, *Scientific Data*, 2, 150066, <https://doi.org/10.1038/sdata.2015.66>, 2015.

999 Gentine, P., Green, J. K., Gu erin, M., Humphrey, V., Seneviratne, S. I., Zhang, Y., and Zhou, S.: Coupling between  
1000 the terrestrial carbon and water cycles-a review, *Environmental Research Letters*, 14, 083003,  
1001 <http://dx.doi.org/10.1088/1748-9326/ab22d6>, 2019.

1002 Ghilain, N., Arboleda, A., and Gellens-Meulenberghs, F.: Evapotranspiration modelling at large scale using near-real  
1003 time MSG SEVIRI derived data, *Hydrology and Earth System Sciences*, 15, 771-786, [https://doi.org/10.5194/hess-  
1004 15-771-2011](https://doi.org/10.5194/hess-15-771-2011), 2011.

1005 Haddeland, I., Heinke, J., Biemans, H., Eisner, S., Fl orke, M., Hanasaki, N., Konzmann, M., Ludwig, F., Masaki, Y.,  
1006 Schewe, J., Stacke, T., Tessler, Z. D., Wada, Y., and Wisser, D.: Global water resources affected by human  
1007 interventions and climate change, *Proceedings of the National Academy of Sciences*, 111, 3251,  
1008 <https://doi.org/10.1073/pnas.1222475110>, 2014.

1009 Helgason, W., and Pomeroy, J.: Problems Closing the Energy Balance over a Homogeneous Snow Cover during  
1010 Midwinter, *Journal of Hydrometeorology*, 13, 557-572, <https://doi.org/10.1175/JHM-D-11-0135.1>, 2012.

1011 Henderson-Sellers, B.: A new formula for latent heat of vaporization of water as a function of temperature, *Quarterly  
1012 Journal of the Royal Meteorological Society*, 110, 1186-1190, <https://doi.org/10.1002/qj.49711046626>, 1984.

1013 Hofste, R. W.: Comparative analysis among near-operational evapotranspiration products for the Nile basin based on  
1014 earth observations first steps towards an ensemble product, M.Sc. Thes, Delft University of Technology, the  
1015 Netherlands, 2014.

1016 Hu, G., Jia, L., and Menenti, M.: Comparison of MOD16 and LSA-SAF MSG evapotranspiration products over  
1017 Europe for 2011, *Remote Sensing of Environment*, 156, 510-526, <https://doi.org/10.1016/j.rse.2014.10.017>, 2015.

1018 Huffman, G. J., Adler, R. F., Arkin, P., Chang, A., Ferraro, R., Gruber, A., Janowiak, J., McNab, A., Rudolf, B., and  
1019 Schneider, U.: The Global Precipitation Climatology Project (GPCP) combined precipitation dataset, *Bulletin of the  
1020 American Meteorological Society*, 78, 5-20, [https://doi.org/10.1175/1520-0477\(1997\)078<0005:TGPCPG>2.0.CO;2](https://doi.org/10.1175/1520-0477(1997)078<0005:TGPCPG>2.0.CO;2),  
1021 1997.

1022 Jia, Z., Liu, S., Xu, Z., Chen, Y., and Zhu, M.: Validation of remotely sensed evapotranspiration over the Hai River  
1023 Basin, China, *Journal of Geophysical Research*, 17, 1-21, <https://doi.org/10.1029/2011JD017037>, 2012.

---

1024 Jiménez, C., Prigent, C., and Aires, F.: Toward an estimation of global land surface heat fluxes from multisatellite  
1025 observations, *Journal of Geophysical Research: Atmospheres*, 114, <https://doi.org/10.1029/2008jd011392>, 2009.

1026 Kim, H. W., Hwang, K., Mu, Q., Lee, S. O., and Choi, M.: Validation of MODIS 16 global terrestrial  
1027 evapotranspiration products in various climates and land cover types in Asia, *Journal of Civil Engineering*, 16, 229-  
1028 238, <https://doi.org/10.1007/s12205-012-0006-1>, 2012.

1029 Leuning, R., Zhang, Y. Q., Rajaud, A., Cleugh, H., and Tu, K.: A simple surface conductance model to estimate  
1030 regional evaporation using MODIS leaf area index and the Penman-Monteith equation, *Water Resources Research*,  
1031 44, <https://dx.doi.org/10.1029/2007wr006562>, 2008.

1032 Li, S., Wang, G., Sun, S., Chen, H., Bai, P., Zhou, S., Huang, Y., Wang, J., and Deng, P.: Assessment of Multi-Source  
1033 Evapotranspiration Products over China Using Eddy Covariance Observations, *Remote Sensing*, 10, 1692,  
1034 <https://doi.org/10.3390/rs10111692>, 2018.

1035 Liu, S. M., Xu, Z. W., Zhu, Z. L., Jia, Z. Z., and Zhu, M. J.: Measurements of evapotranspiration from eddy-covariance  
1036 systems and large aperture scintillometers in the Hai River Basin, China, *Journal of Hydrology*, 487, 24-38,  
1037 <https://doi.org/10.1016/j.jhydrol.2013.02.025>, 2013.

1038 Lu, Y., Cai, H., Jiang, T., Sun, S., Wang, Y., Zhao, J., Yu, X., and Sun, J.: Assessment of global drought propensity  
1039 and its impacts on agricultural water use in future climate scenarios, *Agricultural and Forest Meteorology*, 278,  
1040 107623, <https://doi.org/10.1016/j.agrformet.2019.107623>, 2019.

1041 Ma, N., Szilagyi, J., Zhang, Y., and Liu, W.: Complementary-Relationship-Based Modeling of Terrestrial  
1042 Evapotranspiration Across China During 1982–2012: Validations and Spatiotemporal Analyses, *Journal of*  
1043 *Geophysical Research: Atmospheres*, 124, 4326-4351, <https://doi.org/10.1029/2018jd029850>, 2019.

1044 Majazi, N., Mannaerts, C., Ramoelo, A., Mathieu, R., Mudau, A., and Verhoef, W.: An intercomparison of satellite-  
1045 based daily evapotranspiration estimates under different eco-climatic regions in South Africa, *Remote Sensing*, 9, 307,  
1046 <https://doi.org/10.3390/rs9040307>, 2017.

1047 Martens, B., Miralles, D. G., Lievens, H., van der Schalie, R., de Jeu, R. A. M., Fernández-Prieto, D., Beck, H. E.,  
1048 Dorigo, W. A., and Verhoest, N. E. C.: GLEAM v3: satellite-based land evaporation and root-zone soil moisture,  
1049 *Geoscientific Model Development*, 10, 1903-1925, <https://doi.org/10.5194/gmd-10-1903-2017>, 2017.

1050 McCabe, M. F., Ershadi, A., Jimenez, C., Miralles, D. G., Michel, D., and Wood, E. F.: The GEWEX LandFlux  
1051 project: evaluation of model evaporation using tower-based and globally gridded forcing data, *Geoscientific Model*  
1052 *Development*, 9, 283-305, <https://doi.org/10.5194/gmd-9-283-2016>, 2016.

1053 McNally, A., Arsenault, K., Kumar, S., Shukla, S., Peterson, P., Wang, S., Funk, C., Peters-Lidard, C. D., and Verdin,  
1054 J. P.: A land data assimilation system for sub-Saharan Africa food and water security applications, *Scientific Data*, 4,  
1055 170012, <https://doi.org/10.1038/sdata.2017.12>, 2017.

1056 Michel, D., Jiménez, C., Miralles, D. G., Jung, M., Hirschi, M., Ershadi, A., Martens, B., McCabe, M. F., Fisher, J.  
1057 B., Mu, Q., Seneviratne, S. I., Wood, E. F., and Fernández-Prieto, D.: The WACMOS-ET project – Part 1: Tower-  
1058 scale evaluation of four remote-sensing-based evapotranspiration algorithms, *Hydrology and Earth System Sciences*,  
1059 20, 803-822, <https://doi.org/10.5194/hess-20-803-2016>, 2016.

1060 Miralles, D. G., De Jeu, R. A. M., Gash, J. H., Holmes, T. R. H., and Dolman, A. J.: Magnitude and variability of land  
1061 evaporation and its components at the global scale, *Hydrology and Earth System Sciences*, 15, 967-981,  
1062 <https://doi.org/10.5194/hess-15-967-2011>, 2011a.

1063 Miralles, D. G., Holmes, T. R. H., De Jeu, R. A. M., Gash, J. H., Meesters, A. G. C. A., and Dolman, A. J.: Global  
1064 land-surface evaporation estimated from satellite-based observations, *Hydrology and Earth System Sciences*, 15, 453-  
1065 469, <https://doi.org/10.5194/hess-15-453-2011>, 2011b.

1066 Mu, Q., Zhao, M., and Running, S. W.: Improvements to a MODIS global terrestrial evapotranspiration algorithm,  
1067 *Remote Sensing of Environment*, 115, 1781-1800, <https://doi.org/10.1016/j.rse.2011.02.019>, 2011.

1068 Mu, Q., Zhao, M., and Steven, W.: Running and Numerical Terradynamic Simulation Group: MODIS Global  
1069 Terrestrial Evapotranspiration (ET) Product MOD16A2 Collection 5, 2014a.

1070 Mu, Q., Zhao, M., and Steven, W.: MODIS Global Terrestrial Evapotranspiration (ET) Product MOD16A2 Collection  
1071 5, 2014b.

1072 Mueller, B., Hirschi, M., Jimenez, C., Ciais, P., Dirmeyer, P. A., Dolman, A. J., Fisher, J. B., Jung, M., Ludwig, F.,  
1073 Maignan, F., Miralles, D. G., McCabe, M. F., Reichstein, M., Sheffield, J., Wang, K., Wood, E. F., Zhang, Y., and  
1074 Seneviratne, S. I.: Benchmark products for land evapotranspiration: LandFlux-EVAL multi-data set synthesis,  
1075 *Hydrology and Earth System Sciences*, 17, 3707-3720, <https://doi.org/10.5194/hess-17-3707-2013>, 2013.

1076 Munia, H., Guillaume, J. H. A., Mirumachi, N., Porkka, M., Wada, Y., and Kumm, M.: Water stress in global  
1077 transboundary river basins: significance of upstream water use on downstream stress, *Environmental Research Letters*,  
1078 11, 014002, <https://dx.doi.org/10.1088/1748-9326/11/1/014002>, 2016.

1079 Naumann, G., Alfieri, L., Wyser, K., Mentaschi, L., Betts, R. A., Carrao, H., Spinoni, J., Vogt, J., and Feyen, L.:  
1080 Global Changes in Drought Conditions Under Different Levels of Warming, *Geophysical Research Letters*, 45, 3285-  
1081 3296, <https://doi.org/10.1002/2017gl076521>, 2018.

1082 Oki, T., and Kanae, S.: Global hydrological cycles and world water resources, *Science*, 313, 1068-1072,  
1083 <https://doi.org/10.1126/science.1128845>, 2006.

1084 Pan, S., Tian, H., Dangal, S. R. S., Yang, Q., Yang, J., Lu, C., Tao, B., Ren, W., and Ouyang, Z.: Responses of global  
1085 terrestrial evapotranspiration to climate change and increasing atmospheric CO<sub>2</sub> in the 21st century, *Earth's Future*,  
1086 3, 15-35, <https://doi.org/10.1002/2014ef000263>, 2015.

1087 Reichstein, M., Falge, E., Baldocchi, D., Papale, D., Aubinet, M., Berbigier, P., Bernhofer, C., Buchmann, N.,  
1088 Gilmanov, T., Granier, A., Grünwald, T., Havránková, K., Ilvesniemi, H., Janous, D., Knohl, A., Laurila, T., Lohila,  
1089 A., Loustau, D., Matteucci, G., Meyers, T., Miglietta, F., Ourcival, J.-M., Pumpanen, J., Rambal, S., Rotenberg, E.,  
1090 Sanz, M., Tenhunen, J., Seufert, G., Vaccari, F., Vesala, T., Yakir, D., and Valentini, R.: On the separation of net  
1091 ecosystem exchange into assimilation and ecosystem respiration: review and improved algorithm, *Global Change*  
1092 *Biology*, 11, 1424-1439, <https://doi.org/10.1111/j.1365-2486.2005.001002.x>, 2005.

1093 Revelli, R., and Porporato, A.: Ecohydrological model for the quantification of ecosystem services provided by urban  
1094 street trees, *Urban Ecosystems*, 21, 489-504, <https://dx.doi.org/10.1007/s11252-018-0741-2>, 2018.

1095 Rodell, M., Houser, P. R., Jambor, U., Gottschalck, J., Mitchell, K., Meng, C.-J., Arsenault, K., Cosgrove, B.,  
1096 Radakovich, J., Bosilovich, M., Entin, J. K., Walker, J. P., Lohmann, D., and Toll, D.: The Global Land Data  
1097 Assimilation System, *Bulletin of the American Meteorological Society*, 85, 381-394, [https://doi.org/10.1175/bams-](https://doi.org/10.1175/bams-85-3-381)  
1098 [85-3-381](https://doi.org/10.1175/bams-85-3-381), 2004.

1099 Rodell, M., Beaudoin, H. K., L'Ecuyer, T. S., Olson, W. S., Famiglietti, J. S., Houser, P. R., Adler, R., Bosilovich,  
1100 M. G., Clayson, C. A., Chambers, D., Clark, E., Fetzer, E. J., Gao, X., Gu, G., Hilburn, K., Huffman, G. J., Lettenmaier,  
1101 D. P., Liu, W. T., Robertson, F. R., Schlosser, C. A., Sheffield, J., and Wood, E. F.: The Observed State of the Water  
1102 Cycle in the Early Twenty-First Century, *Journal of Climate*, 28, 8289-8318, [https://doi.org/10.1175/jcli-d-14-](https://doi.org/10.1175/jcli-d-14-00555.1)  
1103 [00555.1](https://doi.org/10.1175/jcli-d-14-00555.1), 2015.

1104 Savoca, M. E., Senay, G. B., Maupin, M. A., Kenny, J. F., and Perry, C. A.: Actual evapotranspiration modeling using  
1105 the operational Simplified Surface Energy Balance (SSEBop) approach, U.S. Geological Survey Scientific  
1106 Investigations Report 2013-126, 16 p, 2013.

1107 Schaffrath, D., and Bernhofer, C.: Variability and distribution of spatial evapotranspiration in semi arid Inner  
1108 Mongolian grasslands from 2002 to 2011, *SpringerPlus*, 2, 547, <https://doi.org/10.1186/2193-1801-2-547>, 2013.

1109 Scheff, J., and Frierson, D. M. W.: Scaling Potential Evapotranspiration with Greenhouse Warming, *Journal of*  
1110 *Climate*, 27, 1539-1558, <https://doi.org/10.1175/jcli-d-13-00233.1>, 2014.

1111 Scott, C. A., Silva-Ochoa, P., Florencio-Cruz, V., and Wester, P.: Competition for Water in the Lerma-Chapala Basin,  
1112 in: *The Lerma-Chapala Watershed: Evaluation and Management*, edited by: Hansen, A. M., and van Afferden, M.,  
1113 Springer US, Boston, MA, 291-323, 2001.

1114 Senay, G., Budde, M., Verdin, J., and Melesse, A.: A coupled remote sensing and simplified surface energy balance  
1115 approach to estimate actual evapotranspiration from irrigated fields, *Sensors*, 7, 979-1000,  
1116 <https://doi.org/10.3390/s7060979>, 2007.

1117 Senay, G. B., Budde, M. E., and Verdin, J. P.: Enhancing the Simplified Surface Energy Balance (SSEB) approach  
1118 for estimating landscape ET: Validation with the METRIC model, *Agricultural Water Management*, 98, 606-618,  
1119 <https://doi.org/10.1016/j.agwat.2010.10.014>, 2011.

1120 Senay, G. B., Bohms, S., and Verdin, J. P.: Remote sensing of evapotranspiration for operational drought monitoring  
1121 using principles of water and energy balance, in: *USGS Staff - Published Research*. 979, 2012.

1122 Senay, G. B., Bohms, S., Singh, R. K., Gowda, P. H., Velpuri, N. M., Alemu, H., and Verdin, J. P.: Operational  
1123 evapotranspiration mapping using remote sensing and weather datasets: A new parameterization for the SSEB  
1124 approach, *Journal of the American Water Resources Association*, 49, 577-591, <https://doi.org/10.1111/jawr.12057>,  
1125 2013.

1126 Senay, G. B., and Kagone, S.: Daily SSEBop Evapotranspiration: U. S. Geological Survey Data Release,  
1127 <https://doi.org/10.5066/P9L2YMV>, 2019.

1128 Senay, G. B., Kagone, S., and Velpuri, N. M.: Operational Global Actual Evapotranspiration: Development,  
1129 Evaluation, and Dissemination, *Sensors*, 20, 1915, <https://doi.org/10.3390/s20071915>, 2020.

1130 Sheffield, J., Wood, E. F., and Roderick, M. L.: Little change in global drought over the past 60 years, *Nature*, 491,  
1131 435-438, <https://doi.org/10.1038/nature11575>, 2012.

1132 Sörensson, A. A., and Ruscica, R. C.: Intercomparison and Uncertainty Assessment of Nine Evapotranspiration  
1133 Estimates Over South America, *Water Resources Research*, 54, 2891-2908, <https://doi.org/10.1002/2017wr021682>,  
1134 2018.

1135 Spinoni, J., Barbosa, P., De Jager, A., McCormick, N., Naumann, G., Vogt, J. V., Magni, D., Masante, D., and  
1136 Mazzeschi, M.: A new global database of meteorological drought events from 1951 to 2016, *Journal of Hydrology:*  
1137 *Regional Studies*, 22, 100593, <https://doi.org/10.1016/j.ejrh.2019.100593>, 2019.

1138 Su, Z.: The Surface Energy Balance System (SEBS) for estimation of turbulent heat fluxes, *Hydrology and Earth*  
1139 *System Sciences*, 6, 85-99, <https://doi.org/10.5194/hess-6-85-2002>, 2002.

1140 Tang, R., Shao, K., Li, Z.-L., Wu, H., Tang, B.-H., Zhou, G., and Zhang, L.: Multiscale validation of the 8-day MOD16  
1141 evapotranspiration product using flux data collected in China, *Journal of Selected Topics in Applied Earth*  
1142 *Observations and Remote Sensing*, 8, 1478-1486, <https://doi.org/10.1109/JSTARS.2015.2420105>, 2015.

1143 Taylor, K. E.: Summarizing multiple aspects of model performance in a single diagram, *Journal of Geophysical*  
1144 *Research*, 106, 7183-7192, <https://doi.org/10.1029/2000JD900719>, 2001.

1145 Trambauer, P., Dutra, E., Maskey, S., Werner, M., Pappenberger, F., van Beek, L. P. H., and Uhlenbrook, S.:  
1146 Comparison of different evaporation estimates over the African continent, *Hydrology and Earth System Sciences*, 18,  
1147 193-212, <https://doi.org/10.5194/hess-18-193-2014>, 2014.

1148 Trenberth, K. E., Smith, L., Qian, T., Dai, A., and Fasullo, J.: Estimates of the Global Water Budget and Its Annual  
1149 Cycle Using Observational and Model Data, *Journal of Hydrometeorology*, 8, 758-769,  
1150 <https://doi.org/10.1175/jhm600.1>, 2007.

1151 UNEP: World atlas of desertification, United Nations Environment Programme, 1997.

1152 Velpuri, N. M., Senay, G. B., Singh, R. K., Bohms, S., and Verdin, J. P.: A comprehensive evaluation of two MODIS  
1153 evapotranspiration products over the conterminous United States: Using point and gridded FLUXNET and water  
1154 balance ET, *Remote Sensing of Environment*, 139, 35-49, <https://doi.org/10.1016/j.rse.2013.07.013>, 2013.

1155 Vinukollu, R. K., Meynadier, R., Sheffield, J., and Wood, E. F.: Multi-model, multi-sensor estimates of global  
1156 evapotranspiration: climatology, uncertainties and trends, *Hydrological Processes*, 25, 3993-4010,  
1157 <https://dx.doi.org/10.1002/hyp.8393>, 2011a.

1158 Vinukollu, R. K., Wood, E. F., Ferguson, C. R., and Fisher, J. B.: Global estimates of evapotranspiration for climate  
1159 studies using multi-sensor remote sensing data: Evaluation of three process-based approaches, *Remote Sensing of*  
1160 *Environment*, 115, 801-823, <https://dx.doi.org/10.1016/j.rse.2010.11.006>, 2011b.

1161 Walter, I. A., Allen, R. G., Elliott, R., Jensen, M. E., Itenfisu, D., Mecham, B., Howell, T. A., Snyder, R., Brown, P.,  
1162 Echings, S., Spofford, T., Hattendorf, M., Cuenca, R. H., Wright, J. L., and Martin, D.: ASCE's Standardized  
1163 Reference Evapotranspiration Equation, in: *Watershed Management and Operations Management 2000*, 1-11, 2001.

1164 Wang, K., and Dickinson, R. E.: A review of global terrestrial evapotranspiration: Observation, modeling,  
1165 climatology, and climatic variability, *Reviews of Geophysics*, 50, <https://doi.org/10.1029/2011rg000373>, 2012.

1166 Waring, R. H., and Running, S. W.: CHAPTER 10 - Advances in Eddy-Flux Analyses, *Remote Sensing, and Evidence*  
1167 *of Climate Change*, in: *Forest Ecosystems, Third Edition ed.*, edited by: Waring, R. H., and Running, S. W., Academic  
1168 Press, San Diego, 317-344, 2007a.

1169 Waring, R. H., and Running, S. W.: Chapter 2 - Water Cycle, in: *Forest Ecosystems, Third Edition ed.*, edited by:  
1170 Waring, R. H., and Running, S. W., Academic Press, San Diego, 19-57, 2007b.

1171 Weerasinghe, I., Bastiaanssen, W., Mul, M., Jia, L., and van Griensven, A.: Can we trust remote sensing  
1172 evapotranspiration products over Africa?, *Hydrology and Earth System Sciences*, 24, 1565-1586,  
1173 <https://doi.org/10.5194/hess-24-1565-2020>, 2020.

1174 Wu, B., Tian, F., Zhang, M., Zeng, H., and Zeng, Y.: Cloud services with big data provide a solution for monitoring  
1175 and tracking sustainable development goals, *Geography and Sustainability*, 1, 25-32,  
1176 <https://doi.org/10.1016/j.geosus.2020.03.006>, 2020.

1177 Xu, T., Guo, Z., Xia, Y., Ferreira, V. G., Liu, S., Wang, K., Yao, Y., Zhang, X., and Zhao, C.: Evaluation of twelve  
1178 evapotranspiration products from machine learning, remote sensing and land surface models over conterminous  
1179 United States, *Journal of Hydrology*, 578, 124105, <https://doi.org/10.1016/j.jhydrol.2019.124105>, 2019.

1180 Yamamoto, M. K., and Shige, S.: Implementation of an orographic/nonorographic rainfall classification scheme in  
1181 the GSMaP algorithm for microwave radiometers, *Atmospheric Research*, 163, 36-47,  
1182 <https://doi.org/10.1016/j.atmosres.2014.07.024>, 2015.

1183 Yang, H., Luo, P., Wang, J., Mou, C., Mo, L., Wang, Z., Fu, Y., Lin, H., Yang, Y., and Bhatta, L. D.: Ecosystem  
1184 Evapotranspiration as a Response to Climate and Vegetation Coverage Changes in Northwest Yunnan, China, *PLOS*  
1185 *ONE*, 10, e0134795, <https://doi.org/10.1371/journal.pone.0134795>, 2015.

1186 Yang, X., Yong, B., Ren, L., Zhang, Y., and Long, D.: Multi-scale validation of GLEAM evapotranspiration products  
1187 over China via ChinaFLUX ET measurements, *International Journal of Remote Sensing*, 38, 5688-5709,  
1188 <https://doi.org/10.1080/01431161.2017.1346400>, 2017.

1189 Yang, Z., Zhang, Q., and Hao, X.: Evapotranspiration trend and its relationship with precipitation over the loess  
1190 plateau during the last three decades, *Advances in Meteorology*, 1-10, <https://doi.org/10.1155/2016/6809749>, 2016.

---

1191 Zhang, K., Kimball, J. S., Mu, Q., Jones, L. A., Goetz, S. J., and Running, S. W.: Satellite based analysis of northern  
1192 ET trends and associated changes in the regional water balance from 1983 to 2005, *Journal of Hydrology*, 379, 92-  
1193 110, <https://doi.org/10.1016/j.jhydrol.2009.09.047>, 2009.

1194 Zhang, K., Kimball, J. S., Nemani, R. R., and Running, S. W.: A continuous satellite-derived global record of land  
1195 surface evapotranspiration from 1983 to 2006, *Water Resources Research*, 46, <https://doi.org/10.1029/2009wr008800>,  
1196 2010.

1197 Zhang, K., Kimball, J. S., and Running, S. W.: A review of remote sensing based actual evapotranspiration estimation,  
1198 *Wiley Interdisciplinary Reviews: Water*, 3, 834-853, <https://doi.org/10.1002/wat2.1168>, 2016.

1199 Zhang, Y., Kong, D., Gan, R., Chiew, F. H. S., McVicar, T. R., Zhang, Q., and Yang, Y.: Coupled estimation of 500 m  
1200 and 8-day resolution global evapotranspiration and gross primary production in 2002–2017, *Remote Sensing of*  
1201 *Environment*, 222, 165-182, <https://doi.org/10.1016/j.rse.2018.12.031>, 2019.

1202 Zhong, Y., Zhong, M., Mao, Y., and Ji, B.: Evaluation of Evapotranspiration for Exorheic Catchments of China during  
1203 the GRACE Era: From a Water Balance Perspective, *Remote Sensing*, 12, 511,  
1204 <https://dx.doi.org/10.3390/rs12030511>, 2020.

1205 Zomer, R. J., Trabucco, A., Bossio, D. A., and Verchot, L. V.: Climate change mitigation: A spatial analysis of global  
1206 land suitability for clean development mechanism afforestation and reforestation, *Agriculture, Ecosystems &*  
1207 *Environment*, 126, 67-80, <https://doi.org/10.1016/j.agee.2008.01.014>, 2008.

1208